materials

MDPI

Article

Pea Pod Valorization: A Green Processing Route to Obtain Cellulosic Reinforcements for Compression Molded Polylactic Acid Biocomposites

Daniela Negrete-Bolagay [1], Victor H. Guerrero [1,*], Salomé Galeas [1], Jennifer Tejedor [1], Patricia I. Pontón [1] and Anja Dosen [2]

[1] Department of Materials, Escuela Politécnica Nacional, Quito 170525, Ecuador; daniela.negrete@epn.edu.ec (D.N.-B.); salome.galeas@epn.edu.ec (S.G.); jennifer.tejedor@epn.edu.ec (J.T.); patricia.ponton@epn.edu.ec (P.I.P.)

[2] International Centre for Diffraction Data, 12 Campus Blvd, Newtown Square, PA 19073, USA; dosen@icdd.com

* Correspondence: victor.guerrero@epn.edu.ec

Abstract

The valorization of agroindustrial residues represents a sustainable alternative in the production of materials attractive for sustainable technologies. In this work, cellulosic materials were isolated from treated pea pods aiming to obtain highly crystalline, thermally stable reinforcements for biocomposites. Four different treatments were evaluated; two employed 0.5 or 0.75 M oxalic acid (OA) solutions at 90 °C, and two used 5% *w*/*v* KOH solutions after each OA treatment. The cellulosic materials (10, 20 wt.%) were compounded with a polylactic acid (PLA) matrix and polyvinyl alcohol (0, 2.5 wt.%) as a compatibilizer by extrusion. Compression molding was used to obtain samples to study the composite's mechanical and thermal behavior. The cellulosic materials and the composites were characterized by Fourier transform infrared spectroscopy, thermogravimetry, and calorimetry. The composites were also subjected to flexural, thermo-mechanical, and water absorption testing. The cellulosic reinforcements obtained using 0.75 M OA and 0.5 M OA and KOH showed the highest crystallinities (91–92%). In general, 20 wt.% reinforced composites showed lower thermal expansion and higher water absorption than those incorporating 10 wt.% reinforcements. The composites incorporating 10 wt.% of 0.5 M OA treated pea pods exhibited flexural modulus/strength 17/3% higher than that of PLA. The composites incorporating 20 wt.% of 0.5 M OA and KOH-treated pea pods showed the highest flexural modulus/strength, 35/25% higher than that of PLA. These results show that agroresidues treated with low-concentration organic acids can be effectively used to tune the mechanical, thermal, and water absorption behavior of biodegradable composites.

Keywords: cellulose reinforced; extrusion; compression molding; mechanical properties

check for updates

Academic Editor: Philippe Evon

Received: 11 July 2025
Revised: 3 September 2025
Accepted: 18 September 2025
Published: 4 October 2025

Citation: Negrete-Bolagay, D.; Guerrero, V.H.; Galeas, S.; Tejedor, J.; Pontón, P.I.; Dosen, A. Pea Pod Valorization: A Green Processing Route to Obtain Cellulosic Reinforcements for Compression Molded Polylactic Acid Biocomposites. *Materials* **2025**, *18*, 4608. https://doi.org/10.3390/ma18194608

Copyright: © 2025 by the authors. Licensee MDPI, Basel, Switzerland. This article is an open access article distributed under the terms and conditions of the Creative Commons Attribution (CC BY) license (https://creativecommons.org/licenses/by/4.0/).

1. Introduction

Despite their versatility, durability, low cost, and wide array of convenient combinations of mechanical, thermal, and biochemical properties, petroleum-based plastics have tremendously deleterious impacts on the environment. These impacts are related to the pollution associated with their continuously increasing production, extremely slow degradation, deficient waste management, a small portion recycled, little awareness about these problems, and insufficiently effective public policies to mitigate them [1]. Developing a

circular plastic economy constitutes an ideal approach to deal with the potentially negative effects stemming from the use of conventional non-biodegradable plastics. In this economy, renewable resources (e.g., biomass, oils) are used to synthesize biopolymers for product manufacturing. At the end of the intended life of these products, they continue through a planned circular end-of-life scenario, including advanced recycling, composting, and upcycling [2]. Developing thermoplastic biocomposites made using biodegradable bio-based polymers and reinforcements represents a currently viable alternative within this framework. Moreover, these biocomposites can conveniently replace traditional plastics in some applications, particularly if low-cost, widely available, easy-to-process, renewable raw materials and residues are used [3].

Polylactic acid (PLA) is a commercially available biodegradable hydrophobic bio-based polymer with good mechanical strength and stiffness, thermal plasticity, and biocompatibility. Despite its high potential, PLA exhibits some disadvantages, including brittleness, low melt strength, heat distortion temperature, and impact resistance, which limit its suitability for various applications [4]. On the other hand, several particulate and fibrous materials, derived from natural resources, have proved very effective for improving the performance of biopolymers such as PLA, especially considering that many of them have low costs (i.e., kenaf fiber: 0.38 kg/USD) and exhibit high specific strength and stiffness [5,6]. Particularly, cellulose is the most abundant natural biopolymer, which can be obtained from lignocellulosic biomasses, including woody forest resources, and widely available agroindustrial residues [7]. Due to its biocompatibility, low density, high specific modulus, biodegradability, and non-toxicity, cellulose has been considered a good reinforcement for brittle thermoplastic matrices such as PLA, improving the mechanical properties of the resulting biocomposites [8–10]. Additionally, productivity and cost competitiveness can be increased if these materials are processed using high-throughput, well-established manufacturing techniques such as extrusion, compression, injection, and blow molding. Likewise, if these biocomposites can be adequately managed at the end of their useful life and are biodegradable, recyclable, or compostable, their environmental impact could be minimized while increasing their lifecycle efficiency [11].

Several cellulosic materials have been used as biocomposite reinforcements, including wood powder, natural fibers, lignocellulosic particles [12], and nanosized cellulose [13]. Recent advances in PLA-based biocomposites have focused on the incorporation of plant-derived cellulosic reinforcements, often sourced from agricultural residues such as sugarcane bagasse, pineapple leaves, water hyacinth, and cereal straws [14–17]. Reinforcements vary in size and morphology, ranging from microparticles to nanofibers and nanocrystals, with loadings typically below 20 wt.% [18,19]. High cellulose content is generally preferred for improving reinforcement yields and enhancing the mechanical performance of the biocomposites. Nanocellulose becomes a good option for various applications since it is possible to improve the biocomposite processability and mechanical performance using smaller reinforcement amounts. However, nanocellulose production requires energy-intensive chemical and mechanical treatments with significant environmental impacts [20]. Moreover, effective dispersion in the matrix is critical, with strategies including the use of polyethylene glycol carriers or surface functionalization of nanocellulose [21]. Although some recent studies suggest that retaining certain amounts of hemicellulose or lignin in lignocellulosic reinforcements can improve interfacial behavior and water resistance [22], other approaches focus on isolating high-purity cellulose to enhance crystallinity and thermal stability, as pursued in this work. These challenges include the selection of low-cost biomass sources such as agro-industrial residues that can be efficiently treated and the development of high-yield, environmentally friendly processing routes to obtain cellulosic reinforcements [23]. Given the hydrophilicity and limited thermal stability that characterize

cellulosic materials, it is also essential to formulate manufacturing methods that ensure good reinforcement dispersion and low agglomeration, as well as an adequate rheology and limited degradation of the polymeric biocomposite melt [3].

This work aims to use an efficient and economical technique to obtain cellulosic materials that can be effective reinforcements in PLA biocomposites. One of the objectives was to avoid using highly concentrated toxic chemicals, specialized and energy-demanding equipment, and the need for more complicated compounding methods. Pea pods were selected for cellulose extraction due to their relatively high cellulose content, which may reach between 27.3 and 69 wt.%. These values depend on several factors, such as extraction techniques, sample preparation, plant variety, and growing conditions [24–26]. In addition, pea pods show a widespread availability worldwide, with an annual production estimated at 4 million tons, which are often not efficiently utilized [27]. Oxalic acid (OA) was chosen among the organic acids used to obtain cellulose reinforcements since it allows relatively high yields and crystallinities [23]. OA was also combined with an alkaline treatment to isolate cellulose. Even though this extraction process is not completely environmentally friendly, minimizing the concentrations of the acid and the base used reduces the impacts compared to traditional methods. The results obtained show promising valorization alternatives for agroindustrial residues such as pea shells, contributing to global sustainability and fulfilling the principles of the circular economy.

2. Materials and Methods

2.1. Materials

Pea pods (Pisum sativum) were collected from a market located in Toacaso (0°45′0″ S and 78°40′60″ W), province of Cotopaxi, Ecuador. The shells were washed with tap and distilled water to remove impurities. Then, the agroindustrial residue was dried in an oven at 80 °C for 24 h. Finally, the pea pods were ground using a knife mill Thomas Wiley model 3379-K05 (Swedesboro, NJ, USA) and sieved (100 mesh).

2.2. Cellulose Extraction

Four different treatments were used to extract cellulose from ground pea pods. The first two consisted of treating the residues with 1400 mL of oxalic acid (OA) solutions at 0.50 M or 0.75 M, corresponding to ratios of 1.8:1 g OA/g pea pods and 2.7:1 g OA/g pea pods, respectively. The mixtures were heated at 80 °C with constant magnetic stirring for 4 h. These treatments were designated CPP1 and CPP2. The other two treatments, designated CPP3 and CPP4, began with the same OA pretreatment described above and were subsequently treated with 5% (*w*/*v*) KOH solutions as a second step to solubilize the pectin and hemicelluloses remaining in the samples [28,29]. In this step, a ratio of 1.67:1 (g KOH per g of treated biomass) was used. The mixtures were stirred magnetically for 7 h at room temperature. Finally, the resulting materials were washed with distilled water until a neutral pH was reached.

2.3. Preparation of PLA Biocomposites

First, the PLA was dried at 80 °C for 24 h to remove moisture. The biocomposite components were then manually mixed. Two weight percentages of cellulosic reinforcements were used (10 and 20% *w*/*w*), and a compatibilizer, polyvinyl alcohol (PVA), was incorporated at 2.5% *w*/*w*. The amount of PLA matrix (90, 80, 87.5, and 77.5 wt.%) used in the preparation of the compounds was adjusted according to the component percentages, as detailed in Table 1. The homogenized mixtures were compounded using a corotating twin-screw microextruder (AX Plastics, Diadema, Brazil). The extruder has six heating zones, with temperatures set as follows: T_1 = 110 °C (feed zone), T_2 = 150 °C and

T_3 = 150 °C (compression zone), T_4 = 147 °C and T_5 = 147 °C (metering zone), and T_6 = 140 °C in the die. The temperatures fluctuated within ±5 °C. During extrusion, the materials were processed at a screw speed of 140 rpm, with a torque of 15 Nm/cm^2 and a residence time of 2–4 min. The filaments obtained were cut using a pelletizer. This procedure was followed to obtain biocomposite pellets with all the formulations prepared. Table 1 shows these formulations, divided into four groups, according to the type of treatment used to obtain the cellulosic reinforcement.

Table 1. Formulations of the PLA biocomposites studied.

Formulation	Composition (wt.%)			
	PLA	Cellulose Reinforcement	Treatment	PVA Compatibilizer
F0	100	0	-	0
F1	90	10	CPP1 0.5 M of OA	0
F2	80	20		0
F3	87.5	10		2.5
F4	77.5	20		2.5
F5	90	10	CPP2 0.75 M of OA	0
F6	80	20		0
F7	87.5	10		2.5
F8	77.5	20		2.5
F9	90	10	CPP3 0.5 M of OA + 5% of KOH	0
F10	80	20		0
F11	87.5	10		2.5
F12	77.5	20		2.5
F13	90	10	CPP4 0.75 M of OA + 5% of KOH	0
F14	80	20		0
F15	87.5	10		2.5
F16	77.5	20		2.5

The biocomposite pellets were used to prepare testing samples by compression molding. The temperature set in the hot press was 160 °C, the pressure was 1000 psi, and the process lasted 5 min. After the molding process, the fabricated samples were annealed at 120 °C for 4 h. Subsequently, the samples were physically, thermally, and mechanically characterized to evaluate their performance.

2.4. Characterization of Cellulosic Reinforcements and Manufactured Biocomposites

2.4.1. Cellulosic Reinforcements

The composition, structure, and thermal behavior of both raw and treated cellulosic materials were studied. The proximate analysis of the raw pea pod lignocellulosic residues was carried out to determine moisture, ash, and volatile matter contents according to ASTM E872-82(2019) [30]. Fixed carbon was calculated by difference. The lignin (ASTM D1106-21) [31], extractives (ASTM D1107-21) [32], and hemicellulose (ASTM D1109-21) [33] contents in the pea pods were determined according to the given standard methods. Cellulose content was calculated by difference. All the tests were performed in duplicate. Regarding the structure, X-ray diffractograms were obtained using an Aeris Research X-ray Panalytical diffractometer (Malvern Panalytical, Almelo, The Netherlands), using copper K-α radiation (λ = 1.54056 Å) under a 40-kV voltage and 15 mA. The diffraction patterns were analyzed using JADE 9.5 software, applying a structureless whole-pattern fitting approach with Pawley refinement [34]. The background was modeled with a polynomial fit, while peak shape parameters,30 scale, offset, and unit cell parameters were refined.

Peak angles were constrained and not refined. Additionally, JADE allows incorporating amorphous profiles in the WPF refinement using a five-parameter pseudo-Voigt function, and it can estimate amorphous content from the fitted profile when the nominal density value (ρ) is provided. Fourier transform infrared spectroscopy (FTIR) was performed using a Jasco spectrometer (Hachioji, Tokyo, Japan), model FT/IR-6800 type A, scanning from 650 to 4000 cm^{-1} at 2 $mm \cdot s^{-1}$.

Regarding thermal behavior, thermogravimetric analysis (TGA) was carried out using a TA Instruments TGA Q500 analyzer (New Castle, DE, USA). The samples were heated from 25 to 1000 °C at 10 $°C \cdot min^{-1}$ under a nitrogen flow of 40 $mL \cdot min^{-1}$. Differential scanning calorimetry (DSC) thermograms were acquired using a TA Instruments DSC Q2000 calorimeter (New Castle, DE, USA) with a heating rate of 10 $°C \cdot min^{-1}$ from 25 to 400 °C and a nitrogen flow of 50 $mL \cdot min^{-1}$.

2.4.2. Characterization of PLA Biocomposites

The effect of adding the different cellulosic reinforcements obtained into the PLA matrix was evaluated in terms of structural, thermal, mechanical, and water absorption properties. FTIR spectroscopy of the biocomposites was performed using a Jasco FT/IR-6800 type A spectrometer (Hachioji, Tokyo, Japan) with the accessory ATR-PRO-ONE, scanning from 400 to 4000 cm^{-1} at a speed of 2 $mm \cdot s^{-1}$.

The thermal stability of the composites was studied by TGA. Sample weights ranged from 10 to 30 mg. Samples were scanned from 25 to 600 °C at 10 $°C \cdot min^{-1}$, under 40 $mL \cdot min^{-1}$ nitrogen flow. DSC analyses were performed to determine the glass transition (Tg) and melting temperature (Tm) of the biocomposites. All the samples were scanned from 25 to 200 °C at 10 $°C \cdot min^{-1}$, under a nitrogen flow of 40 $mL \cdot min^{-1}$. A single c_c of the composites was determined as follows:

$$c_c = \frac{\Delta H_m}{\Delta H_m^0 \left(1 - m_f\right)} 100\%$$

where ΔH_m^0 is the theoretical value of the melting enthalpy (93 $J \cdot g^{-1}$) for 100% crystalline PLA, ΔH_m is the melting enthalpy for the sample studied, and m_f is the mass fraction of the filler [35,36]. The thermomechanical behavior of the biocomposites was studied using a TA Instruments Q400 TMA analyzer (New Castle, DE, USA). The measurements were carried out in a temperature range from 25 to 120 °C, with a heating rate of 3 $°C \cdot min^{-1}$, and a loading force of 0.05 N.

For the mechanical characterization, flexural tests were performed according to ASTM D790-17 [37]. Five specimens (3.2 × 12.7 × 61 mm) of each biocomposite formulation were tested using a Shimadzu AGS-X universal testing machine (Shimadzu Corporation, Kyoto, Japan), with a test speed of 1.37 $mm \cdot min^{-1}$ and a 51.2 mm distance between supports. The average and standard deviation of the flexural modulus, strength, and strain at failure were calculated for each formulation.

Water absorption tests were carried out according to ASTM D792-20 [38], immersing the specimens in distilled water at 50 °C from 1 to 21 days. At regular time intervals, each specimen was removed from the water immersion bath and wiped with tissue paper to remove surface water and subsequently weighed using an analytic balance. The water absorption was calculated as the percentage increase in the initial weight [39]:

$$Mt(\%) = \frac{(Wt - Wo)}{Wo} 100\%$$

where W_t is the weight of the sample after a given immersion time and W_o is the initial weight of the sample.

3. Results and Discussion

3.1. Characterization of the Cellulosic Reinforcements

3.1.1. Composition and Yield

The cellulose, hemicellulose, lignin, and extractive contents in the raw pea pod shells were 37.81, 34.42, 6.25, and 21.52%, respectively. The proximate analysis showed 84.37, 1.34, 8.77, and 5.52% of volatile matter, fixed carbon, ash, and moisture in the pea pods, respectively. The most convenient process and reagents for cellulose isolation are determined by the availability of lignocellulosic residues, their composition, production scale, and product quality. In this work, the treatment of pea husks for obtaining cellulose was based on using OA and KOH. OA is a dicarboxylic acid in which one or both carboxyl groups can react with the hydroxyl groups of cellulose [40]. OA is abundant, biodegradable, and non-volatile and is considered a sustainable acid. The yield of OA depends on the concentrations and the processing routes (chemical or mechanical), which promote the depolymerization of cellulose, affecting its amorphous regions and leading to high yields of crystalline structures [41]. It is worth noting that OA represents a promising alternative to mineral acids such as H_2SO_4, HCl, H_3PO_4, and HBr, which often cause significant problems, including equipment corrosion, high water consumption, recovery difficulties, and the generation of toxic byproducts [42]. Furthermore, oxalic acid has been shown to exhibit higher selectivity than sulfuric acid, as it promotes more effective hydrolysis of the β-(1,4) bonds present in cellulose [43].

In a study conducted by Xu et al. (2017) [44], the yields and thermal stability achieved in cellulose production were analyzed. The findings indicated that, with oxalic acid, an 85% yield and high thermal stability up to 350 °C were obtained, whereas with sulfuric acid, the yield was 35% and degradation began at 200 °C [44]. Likewise, the use of alkaline treatments (NaOH, LiOH, KOH, $Ca(OH)_2$) has been reported to break the bonds linking lignin and polysaccharides [45]. However, alkaline solutions, especially NaOH, induce cellulose aggregation and, due to their amphiphilic nature, fail to dissolve it. From an environmental perspective, this method is unfavorable, as it requires large amounts of water to neutralize the mixture and remove impurities before subsequent transformations [46].

Therefore, the use of less harmful solvents that reduce wastewater generation is necessary. In this regard, oxalic acid has been employed in the controlled hydrolysis of hemicellulose, preventing cellulose degradation when used at low concentrations [42,43]. Moreover, owing to its low solubility at room temperature, oxalic acid can be easily recovered and reused through a simple crystallization process, thereby improving process sustainability and minimizing environmental impact [47].

In this work, the extraction yields of the cellulosic materials obtained from the CPP1, CPP2, CPP3, and CPP4 treatments were 41.14, 33.63, 22.76, and 22.49% (*w*/*w*), respectively, expressed as a percentage of the initial dry mass of the pea pod shells. These values are similar to the ones reported by previous authors who have employed OA and/or KOH to obtain cellulose. For instance, Romrue et al. (2022) [48] investigated the alkaline extraction of cellulose from rice straw (RS), corn cob (CC), Phulae pineapple leaves (PL), and peels (PP). The procedure was based on the use of 1.4% acidified sodium chlorite (NaClO2) and 5% KOH in all samples. The extraction yields of the cellulose obtained were 32.26, 38.18, 16.60, and 9.05 wt.% for RS, CC, PL, and PP, respectively [48]. It is worth noting that the OA concentration used in this work is relatively low compared to the ones used by previous researchers. For example, cellulose microfibers/nanofibers (CMNF) were obtained from bleached eucalyptus pulp by using 25 wt.% (2.94 M) and 50 wt.% (5.88 M) OA

aqueous solutions [49]. These relatively low acid concentrations improve the environmental friendliness of the treatments while still allowing for good yields. On the other hand, the use of 5% w/v KOH reduces the yield but increases the cellulose content by facilitating the removal of hemicellulose, pectin, and lignin still present after the acid treatment step, as verified by FTIR spectroscopy (see Section 3.1.2). The alkaline treatment breaks down natural fibers into individual fibrils, increasing the accessibility of surface hydroxyl (–OH) groups. These –OH groups act as reactive sites that can form hydrogen bonds with the PLA matrix, improving interfacial adhesion, surface tension, and the wettability of the treated fibers [50–52]. Although excessively aggressive alkaline treatments can partially degrade cellulose chains or reduce crystallinity, our study using a low concentration did not affect the cellulose structure. The materials obtained illustrate the possibility of using relatively low concentrations of OA to obtain effective reinforcements of a biodegradable matrix.

3.1.2. FTIR Analyses

Figure 1 shows the FTIR spectra for the cellulosic materials obtained through the different chemical treatments studied in this work. The region between 3300 and 3200 cm^{-1} was associated with the –OH groups of cellulose [53]. A broad band related to the vibrations of hydroxyl groups was detected around 3390 cm^{-1}. The bands observed around 2900 cm^{-1} represent the characteristic bands of C-H and CH_2 stretching vibrations in cellulose and hemicellulose.

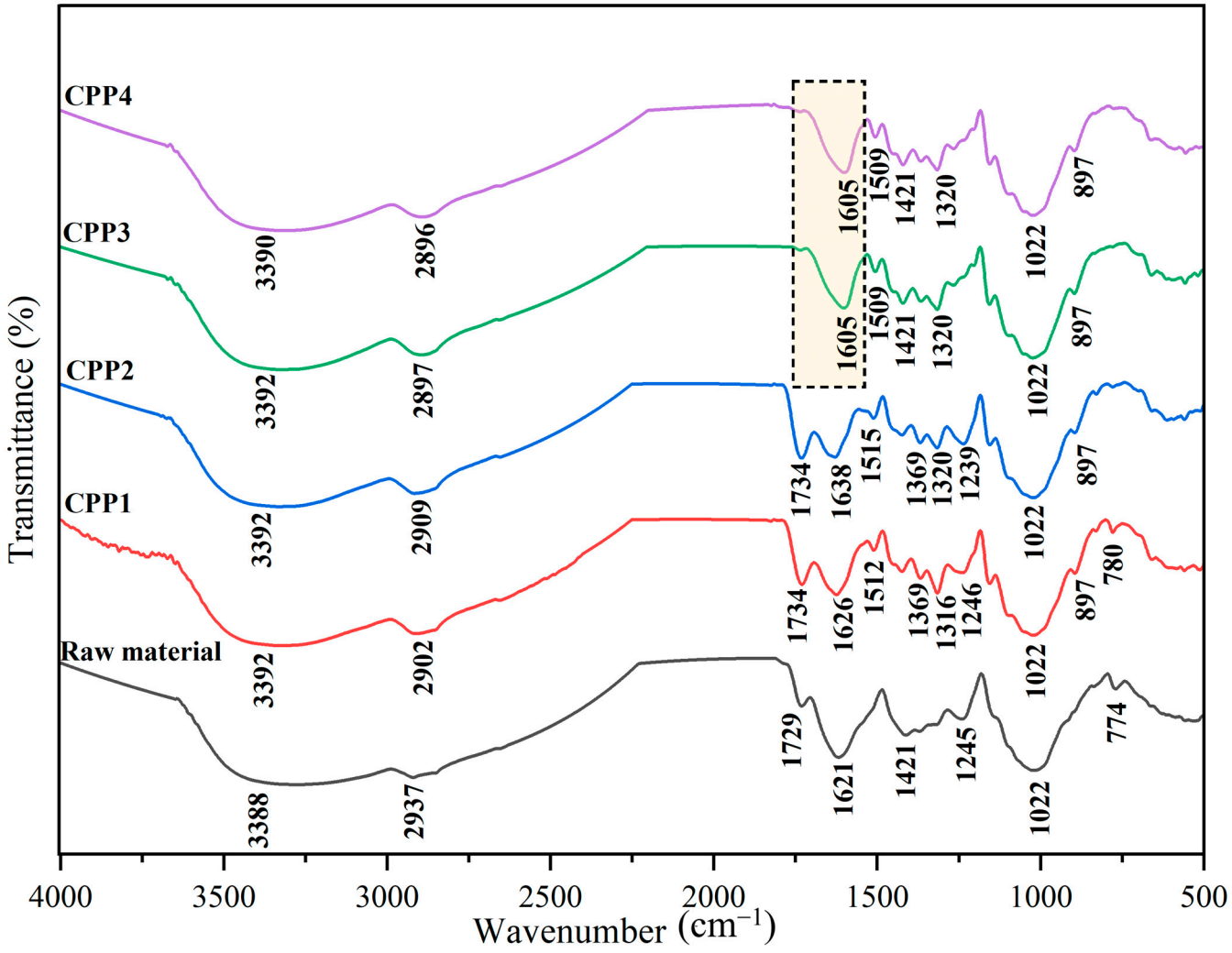


Figure 1. FTIR spectra of cellulosic materials obtained from pea pods by different acid and acid/alkaline treatments.

CPP1 and CPP2 cellulosic materials, observed around 1730 cm^{-1} and 1626 cm^{-1}, were attributed to acetyl-uronic ester groups, ferulic, and p-coumaric acids of lignin and hemicelluloses, respectively [54]. These bands disappeared in the CPP3 and CPP4 spectra, indicating the removal of hemicelluloses and lignin through successive chemical treatments [55,56]. In the FTIR spectrum of the extracted cellulose, the region below 1600 cm^{-1} corresponds to the so-called fingerprint region, which contains characteristic vibrations of cellulose [57]. The band at ~1605 cm^{-1} is attributed to –OH bending of absorbed water. Signals at 1421 and 1369 cm^{-1} correspond to the bending vibrations of C–H and C–O groups associated with residual hemicellulose and lignin, respectively. The band at 1425–1442 cm^{-1}, assigned to CH_2 scissoring, is also recognized as the "crystallinity band" of cellulose I, in agreement with XRD results [58]. The absorptions at 1174 and 1120 cm^{-1} are attributed to asymmetric C–O–C bridge stretching, while the band near 905 cm^{-1} corresponds to β-glycosidic linkages between glucose units [59]. In addition, the peaks at 1022 cm^{-1} (C–O stretching) and 897 cm^{-1} (C–H rocking) further confirm the preservation of the cellulose structure after the chemical treatments, as observed in the CPP3 and CPP4 samples [56].

3.1.3. Crystallinity

The XRD patterns of cellulosic materials obtained from pea pods are shown in Figure 2. The typical pattern of cellulose type I exhibits peaks at 2θ around 15.2, 16.6, and 22.9°, and another main peak at 34.9° [54,60,61]. The cellulosic materials obtained in this work exhibit the same peaks, while the more prominent ones are around 2θ = 14.9° and 22.08°. The similarity of these patterns to those reported for commercial microcrystalline cellulose (MCC), exhibiting peaks at 2θ = 15.4, 16.2, 22.5, and 34.5° [62], indicates that the treatments successfully produced cellulose-rich materials. These diffraction patterns suggest the presence of crystalline cellulose domains, supporting the potential of the extracted materials as reinforcements in composite applications [63].

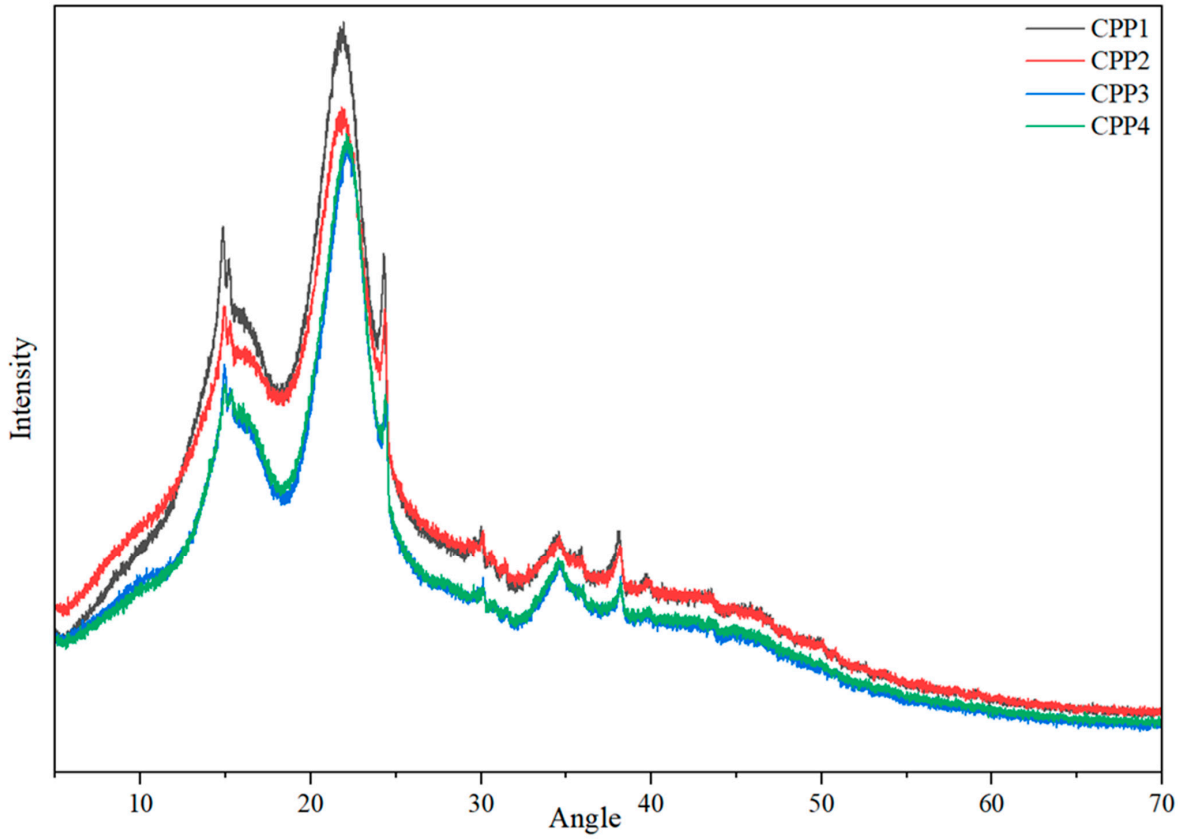


Figure 2. X-ray diffraction (XRD) patterns of the cellulosic materials extracted from pea pods.

Although variations in peak intensities were observed between treatments, the broad nature of the diffraction peaks makes it difficult to visually distinguish crystallinity differences between samples. XRD results provide qualitative confirmation of the presence of crystalline cellulose domains in the extracted materials, supporting their potential use as reinforcement in polymer composites.

Broad cellulose peaks indicate small crystallite size and the presence of an amorphous phase. WPF analysis, performed using the PDF-5+ database [64] entry 00-056-1719, showed that CPP1 and CPP2 contain about 35% amorphous content, whereas CPP3 and CPP4 exhibit significantly higher crystallinity. These results suggest that differences in sample preparation and KOH treatment influence the formation of the amorphous phase. Note that a high crystallinity is desired for improving mechanical properties in composite applications [65], suggesting the potential of CPP2, CPP3, and CPP4 as reinforcements.

3.1.4. Thermogravimetric Analysis

The thermograms obtained for the cellulosic materials studied are shown in Figure 3, while the onset and maximum degradation temperatures are given in Table 2. The thermograms show a mass decrease around 100 °C due to the removal of moisture and some volatile components from the samples [56,61]. Note that the presence of water absorbed in the samples was also determined in the FTIR spectra shown (Figure 1), where a band around 1630 cm^{-1} was observed. This is due to the hydrophilic nature of cellulosic materials. Around 200 and 430 °C, the degradation of cellulose, lignin, and hemicellulose chains was observed. Note that the glucose units begin to decompose into carbon at lower temperatures, while at higher temperatures, these units depolymerize into volatile products [66]. Above 500 °C, products such as CO_2, CO, hydrocarbons, and hydrogen leave the samples [67]. The untreated pea pods exhibited lower degradation temperatures compared to the treated ones. This is due to the presence of lignin and hemicellulose in the raw pea pods. The results obtained after treatment demonstrate that cellulose is thermally stable up to 280 °C, where no significant mass loss was detected. Similar results were observed in the extraction of MCC derived from pea pods, where the T_{onset} was 265 °C, and T_{max} was 340 °C [56].

3.1.5. DSC Analysis

Figure 4 shows details of water evaporation from the cellulose surface and the initial thermal decomposition of the cellulosic materials. DSC analysis revealed a broad endothermic peak around 50–150 °C for all samples, corresponding to the vaporization of the moisture absorbed due to the hydrophilic nature of the hydroxyl surfaces on cellulose [68,69]. Changes in the enthalpy associated were also observed. The enthalpy change is lower for raw pea pods and increases after the treatments. In the case of the endothermic peak, it shifts to a lower temperature compared to the raw pea pods. This could be explained by an increase in the length/diameter ratio of the cellulosic fibers during the KOH treatment, which facilitates the evaporation of moisture [70]. Similar results were observed when cellulose fibers were modified using vinyltrimethoxysilane and maleic anhydride to improve their wettability in the hydrophobic polymeric matrix. In that case, the changes observed by DSC were also attributed to the length/diameter ratio of the fiber [71].

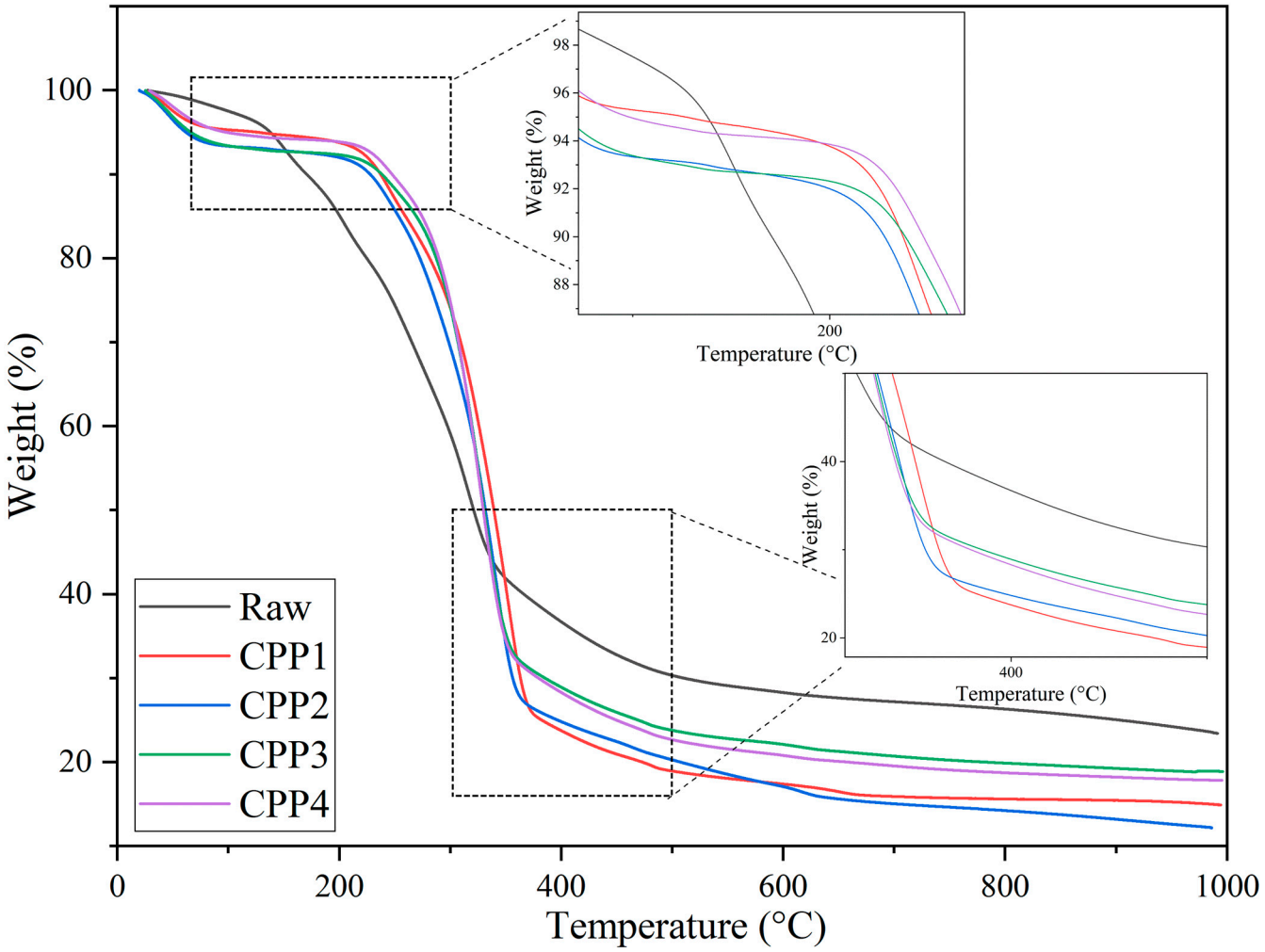


Figure 3. TGA of cellulosic materials obtained after acid and acid/alkaline treatments of pea pod shells.

Table 2. Degradation onset and maximum temperatures, as well as char residues of raw and treated pea pods, determined from TGA analyses.

Samples	Crystallinity Index (%)	T_{onset} °C	T_{max} °C	Char Residue at 800 °C (%)
Raw material	-	227.01	315.77	26.29
CPP1	65.59	283.91	351.60	15.60
CPP2	64.41	283.11	341.30	14.21
CPP3	91.14	285.63	328.37	19.87
CPP4	92.62	284.32	327.93	18.73

Summarizing, FTIR spectroscopy and XRD show that the cellulose obtained through the treatments performed has a type I structure. The acid-alkaline treatments effectively removed hemicelluloses and lignin from the pea pods while preserving the cellulose structure, as shown by FTIR spectroscopy. This also increases the crystallinity of the treated materials, as evidenced by XRD.

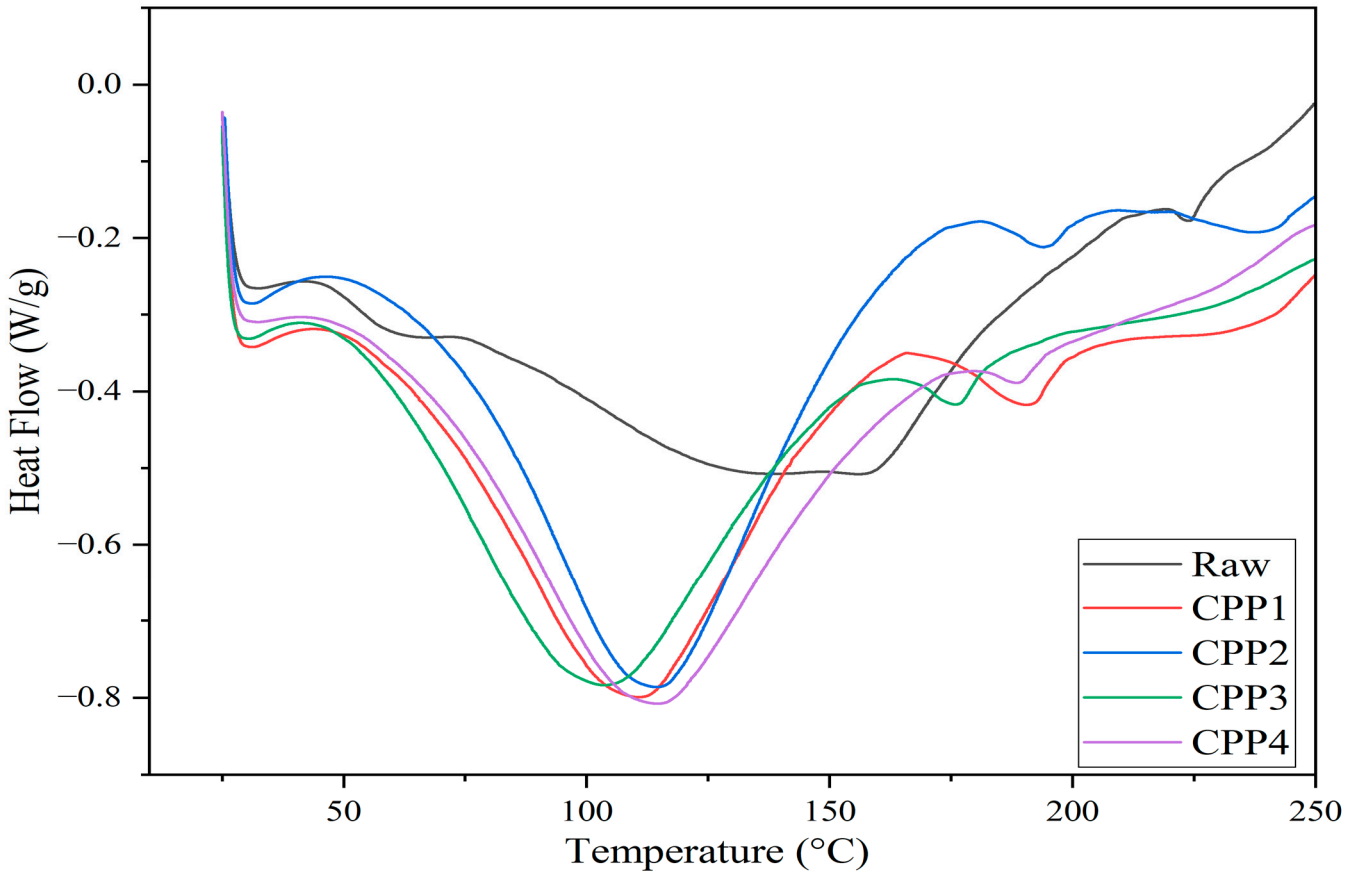


Figure 4. DSC of raw pea pods and treated cellulosic materials.

3.2. Biocomposites Characterization

3.2.1. FTIR Analysis

Figure 5 shows the spectra of the PLA matrix used and the biocomposites formulated in this work. The characteristic absorption bands of pure PLA were observed at 1448, 1187, 1083, and 867 cm^{-1}. The stretching vibration of the C-O groups corresponds to the bands at 1187 and 1083 cm^{-1}. The bands observed at 1448 cm^{-1} could be related to the deformation of carbon-hydrogen (C-H) bonds in the CH_3 group. Likewise, bands at 920 and 867 cm^{-1} appear due to the presence of C-C single bonds [10].

Regardless of the cellulosic reinforcement content, the position of the bands does not change. On the other hand, the bands around 3300 and 2850 cm^{-1} are attributed to the stretching of -OH and -CH groups, characteristic of cellulose. This indicates that the cellulosic reinforcements and the PLA matrix are interacting. In the band at 1743 cm^{-1}, no change was observed after the incorporation of cellulosic reinforcements. This is due to the interaction between the carbonyl group (C-O) of PLA and the hydroxyl groups (-OH) of cellulose [72]. Furthermore, the presence of coupling agents leads to robust and broad peaks around 1080 cm^{-1}, which can be attributed to the CO-O-CO stretching vibration of the compatibilizers. This suggests that a chemical interaction occurs between the cellulose and the coupling agents [73].

In order to complement the qualitative interpretation of the FTIR spectra, a quantitative analysis was performed by calculating the areas of the absorption peaks corresponding to specific vibrational bands (see Table 3). In particular, the area ratios A_{1448}/A_{1743} (associated with CH_3 bending and C=O stretching in PLA, respectively) and A_{867}/A_{1743} (related to C–H rocking in cellulose and C=O stretching in PLA) were determined for all formulations (F0–F16). These ratios remained relatively stable, ranging from 0.21 to 0.27 and 0.060 to

0.086, respectively. This low variability suggests a uniform distribution of the cellulosic reinforcement and indicates that the incorporation of cellulose did not significantly alter the bulk chemical structure of the PLA matrix. Nevertheless, the presence of characteristic peaks and minor variations in band shape and width continue to support the occurrence of molecular interactions between PLA and the cellulosic phases.

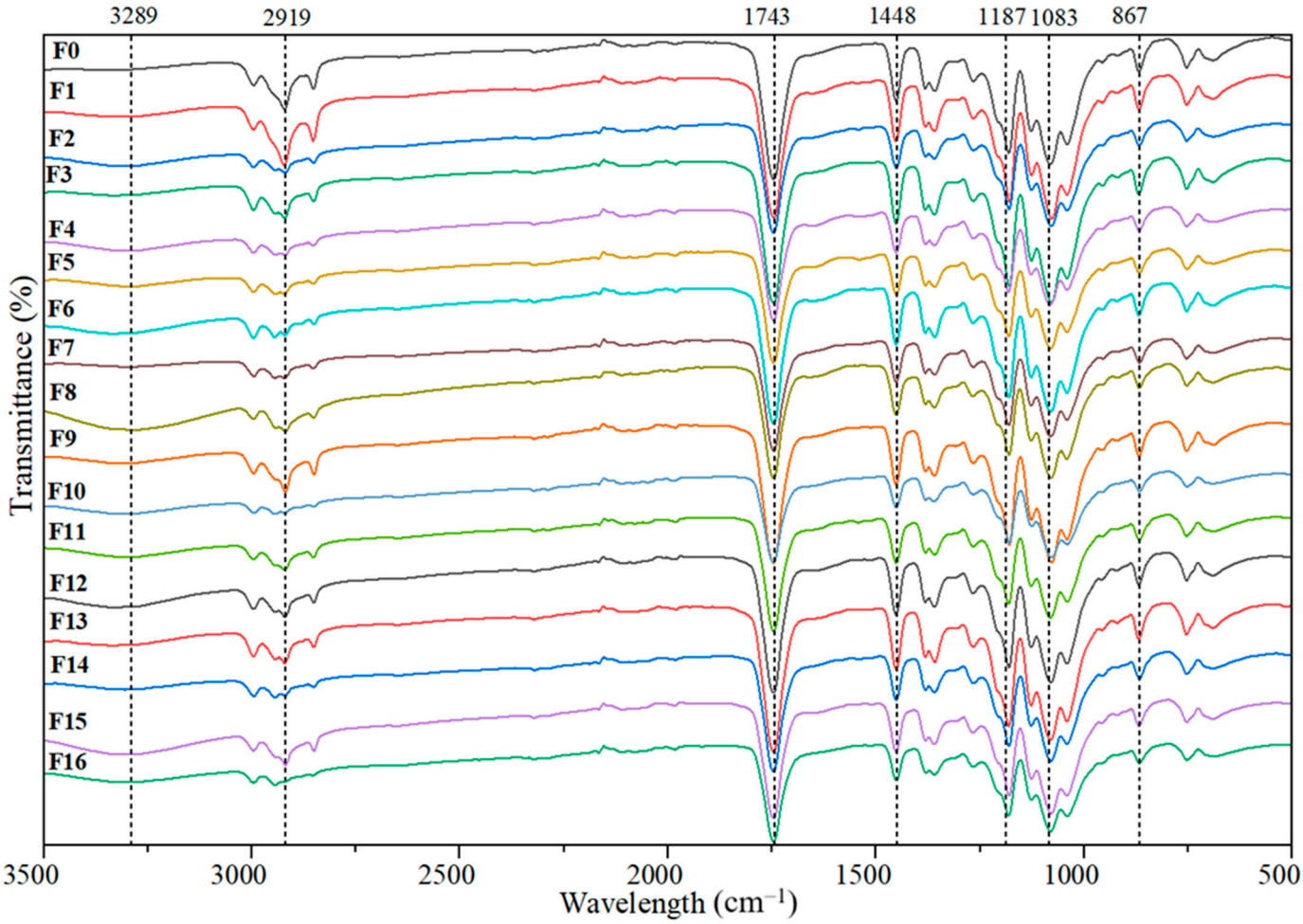


Figure 5. FTIR spectra of the PLA and the biocomposites prepared.

3.2.2. Thermal Analysis

Thermal mass loss curves of the neat PLA and the biocomposites formulated are shown in Figure 6B. The degradation temperatures (T_{d10}, $T_{d50,}$ and T_{d90}) and the residual char fraction at 600 °C are given in Table 4. Note that the degradation onset temperature can be influenced by the type and content of the reinforcement used, relative to pure PLA [74]. PLA was thermally stable up to 320 °C and then began to degrade rapidly in a single step. The loss of 90% of its mass was observed at approximately 460 °C, and there was a 1.4% residue at 600 °C. In contrast, thermal degradation of PLA-CPP cellulose composites initiates at temperatures in the range of 280–300 °C, approximately 10% lower than that of the PLA, leading to rapid weight losses up to 350 °C. This is primarily associated with the thermal degradation of hemicelluloses and cellulose. The degradation temperatures were lower for the biocomposites incorporating OA-KOH-treated pea pods. In a previous study using fibers obtained from sugarcane bagasse in matrices of bioepoxy and unsaturated polyester resins, chemical treatments with alkali, silane, and OA were performed to improve fiber-matrix adhesion and enhance mechanical, thermal, and physical properties. The results showed that the alkali-treated sample exhibited better thermal stability.

However, no significant changes were observed with oxalic acid treatment, resulting in lower stability [75]. Without compatibilizers, the degradation temperatures decreased as the reinforcement content increased from 10 to 20 wt.%. The literature also corroborates that the treatment of cellulose with certain acids (e.g., sulfuric acid) can reduce the thermal stability of CPP celluloses and increase carbon formation at the end of the degradation process [76]. Furthermore, the decrease in the thermal stability of the composites can be attributed to the lower decomposition temperature of cellulose relative to PLA [77]. For example, Tan et al. (2021) reported that the maximum degradation temperature decreased due to the lower initial degradation temperature of microcellulose (MCC), which leads to reduced thermal stability of the composite [78]. Other contributing factors include the agglomeration and poor dispersion of cellulose in the matrix, which accelerate the diffusion of volatile decomposition products and may facilitate the propagation of oxygen in the matrix [79].

Table 3. Quantitative analysis of FTIR absorption peak area ratios for PLA/cellulose composites.

Formulation	A1448/A1743	A867/A1743
F0	0.250	0.0810
F1	0.266	0.0857
F2	0.217	0.0684
F3	0.257	0.0846
F4	0.220	0.0654
F5	0.223	0.0670
F6	0.245	0.0786
F7	0.222	0.0677
F8	0.238	0.0667
F9	0.252	0.0820
F10	0.219	0.0662
F11	0.231	0.0682
F12	0.248	0.0790
F13	0.255	0.0831
F14	0.225	0.0703
F15	0.214	0.0606
F16	0.243	0.0731

Table 4. Thermal degradation of biocomposites with different cellulosic reinforcements.

Sample	T_{d10} (°C)	T_{d50} (°C)	T_{d90} (°C)	Char Residue at 600 °C (%)
F0	331.09	365.5	459.6	1.416
F1	317.7	349.17	367.46	0.702
F2	298.77	335.36	354.39	0.654
F3	302.43	338.25	360.42	0.5629
F4	307.2	342.73	363.02	1.152
F5	311.93	346.06	364.89	0.416
F6	301.25	336.89	356.51	1.310
F7	303.2	337.02	354.9	0.402
F8	302.79	337.85	357.26	0.806
F9	296.64	330.7	349.92	0.593
F10	283.96	313.85	329.73	0.543
F11	286.89	318.79	335	0.801
F12	286.24	319.54	342.95	1.478

Table 4. *Cont.*

Sample	T_{d10} (°C)	T_{d50} (°C)	T_{d90} (°C)	Char Residue at 600 °C (%)
F13	290.11	328.12	346.7	1.83
F14	288.10	325.49	344.48	2.11
F15	284.22	318.22	335.23	0.438
F16	278.48	312.03	336.83	1.156

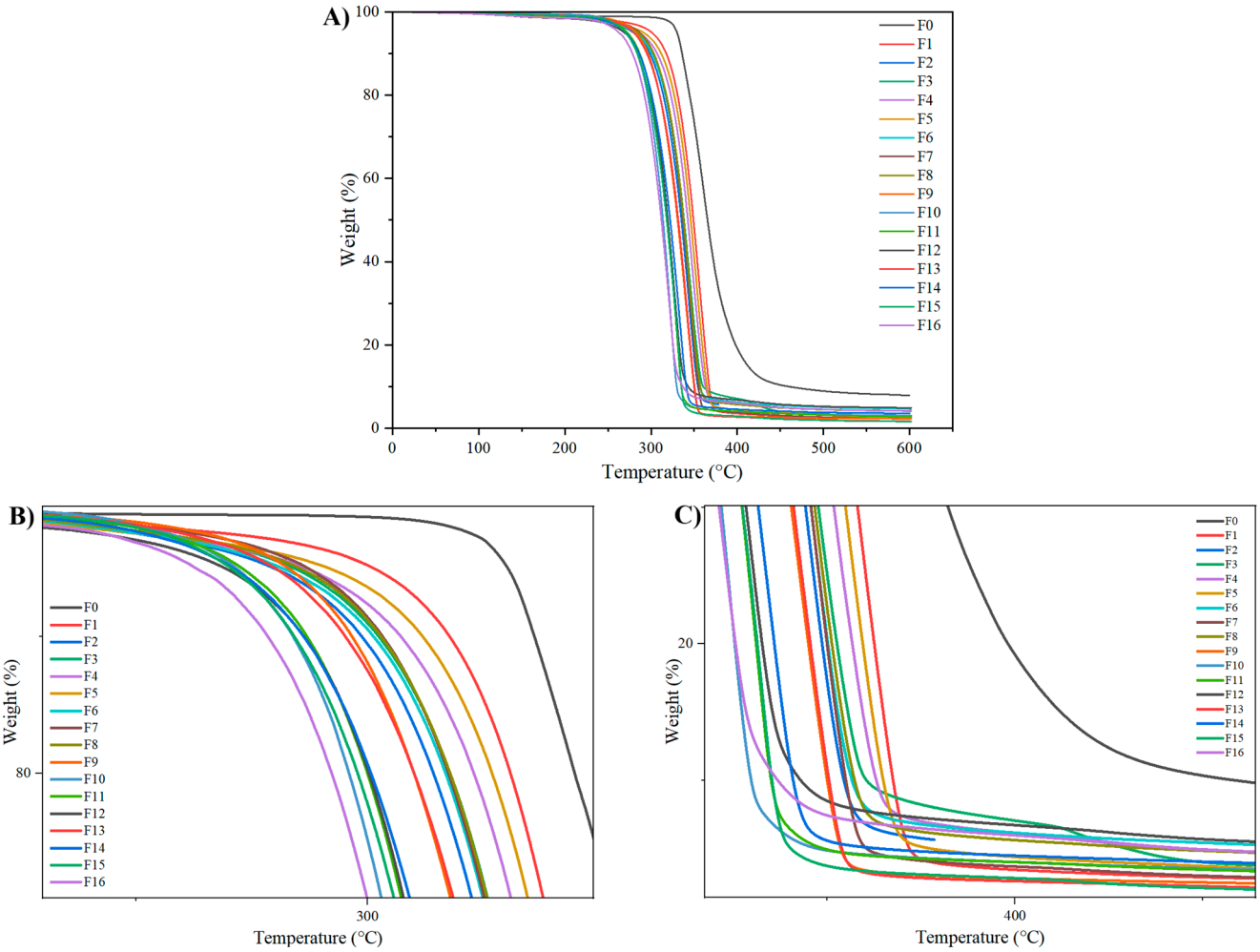


Figure 6. Thermogravimetric analysis of PLA and cellulose reinforced biocomposites. (**A**) complete thermogram; (**B**) initial degradation region, and; (**C**) final degradation region.

3.2.3. DSC Analysis

The DSC thermograms recorded during the first and second heating of the pure PLA and the biocomposites formulated are shown in Figure 7. The data derived from DSC analysis are given in Table 5. Thermograms exhibited a double endothermic melting peak for PLA and the PLA-CPP composites. The appearance of multiple melting peaks is common in many semi-crystalline polymers, and the literature suggests several explanations for this phenomenon, such as the presence of different crystallographic forms, crystalline layers with various thicknesses, and melting and recrystallization co-occurring [80].

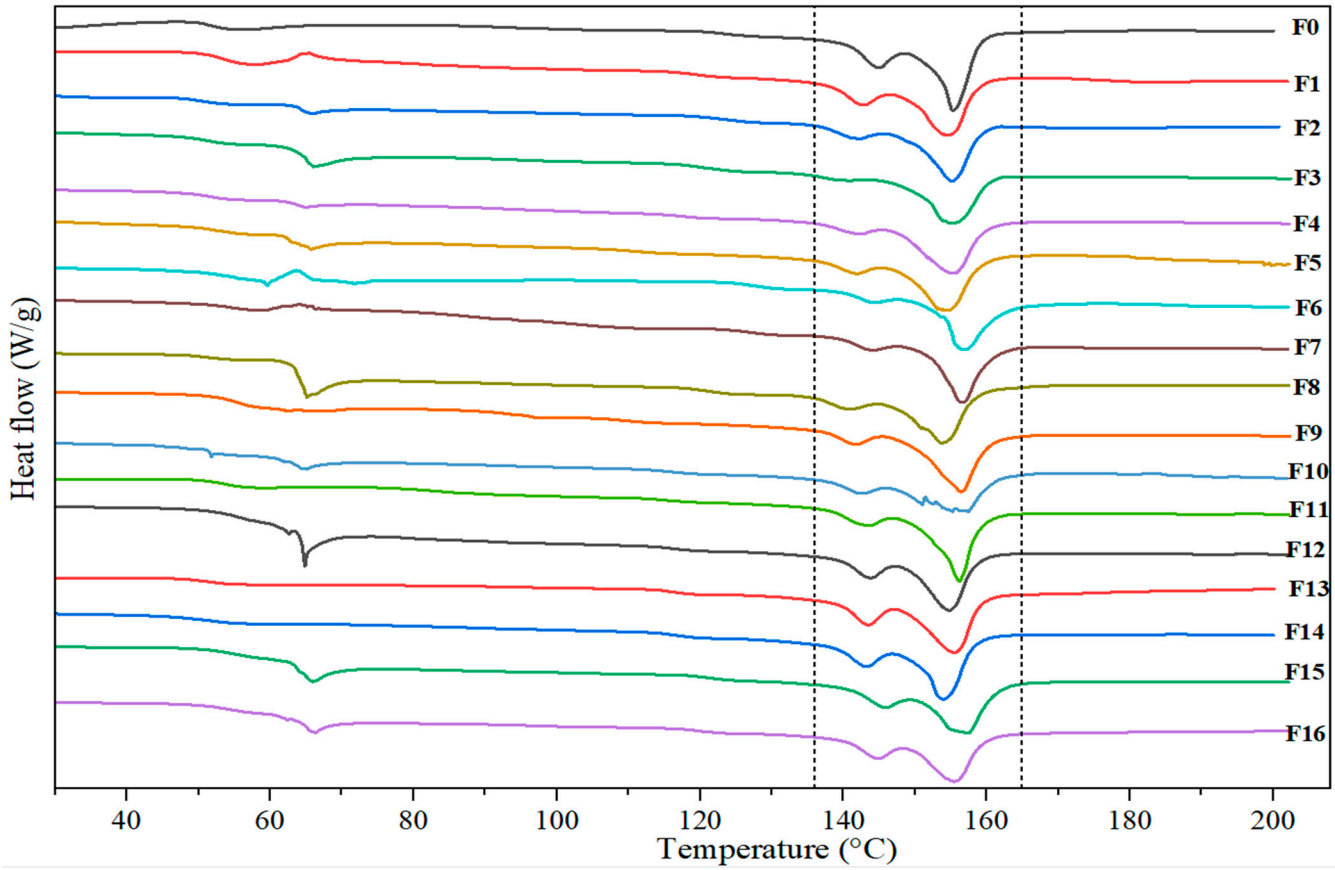


Figure 7. DSC thermograms of the PLA-based composites with different cellulosic content.

Table 5. Thermal properties of PLA and PLA-CPP composites obtained by DSC.

Samples	1st Heating				
	T_g (°C)	T_m (°C)		ΔH_m (J/g)	χ_c (%)
		T_{m1}	T_{m2}		
F0	51.87	140.63	152.96	31.20	33.55
F1	53.46	138.04	149.68	29.28	34.98
F2	50.26	136.46	149.99	22.35	30.04
F3	51.74	134.57	150.52	21.52	27.47
F4	51.94	140.95	148.21	23.97	29.86
F5	53.22	137.08	149.04	25.29	28.64
F6	55.14	139.98	154.02	20.61	33.99
F7	53.99	139.60	152.81	21.93	25.33
F8	51.19	135.83	149.11	25.51	30.43
F9	55.41	137.19	149.66	26.35	30.48
F10	51.68	137.59	150.41	23.99	35.42
F11	53.15	137.89	152.45	25.97	29.48
F12	56.57	139.43	149.60	24.59	36.03
F13	51.75	139.29	149.13	28.51	29.38
F14	51.88	138.57	151.14	25.10	38.32
F15	55.05	141.16	152.01	26.42	32.09
F16	53.87	140.33	150.11	23.89	36.66

During the first heating cycle, the T_g of both the composites and the pure PLA was very similar, ranging between 50 and 55 °C. After T_g, a small endothermic peak was

observed for both pure PLA and its biocomposites, which is a typical effect of physical aging [81,82]. No exothermic cold crystallization peak was detected for the samples annealed at 120 °C for 4 h. Regarding the degree of crystallization, it was higher than 30% for most of the biocomposites. It was also observed that, in general, the crystallinity increased as the reinforcement content went from 10 to 20 wt.%. This can be attributed to the nucleation capacity of the cellulosic reinforcements, which promotes the crystallization of PLA [83]. Additionally, the increase in χ_c was higher for those biocomposites incorporating pea pods treated with OA and KOH. Annealing enhances crystallinity due to PLA's ability to crystallize between its glass transition and melting temperatures, leading to improved mechanical properties. Simmons et al. (2019) [84] developed a strategy to enhance the thermal and mechanical properties of PLA through a reactive extrusion process and the addition of a biofiller as a nucleating agent. The results indicate that annealing at 100 °C increased the crystallinity by 45% and 50% for the developed formulations [84].

3.2.4. TMA Analysis

Figure 8 illustrates the effect of the cellulosic reinforcements on the thermal expansion of the biocomposites. The glass transition ranges from 50 to 56 °C, in which a maximum slope change is identified. The point where this shift change occurs corresponds to the glass transition temperature T_g, which is similar to the one obtained by DSC for the biocomposites studied (see Table 5 and Figure 7). Table 6 lists the coefficients of thermal expansion (CTE) for each PLA and PLA-CPP composite. The pure PLA matrix exhibited a larger dimensional change as the temperature ranged from 25 to 120 °C. This is because the molecular chains within the polymer move vigorously with higher thermal energy, causing the material to expand [85]. In general, an improvement in the dimensional stability of the composites is observed, and their thermal expansion was lower below the T_g. The CTE decreased as the content of cellulosic reinforcement increased. For instance, the CTE decreased from 95.38 for PLA to approximately 50×10^{-6} $1/°C^{-1}$ for the composite F16, reinforced with 20 wt.% cellulose. This behavior is attributed to the interfacial adhesion between the cellulosic reinforcements and the matrix in the biocomposite [86]. In this regard, this behavior is similar to the effect of adding cellulose nanofibers to a PLA matrix, which decreased the CTE by 24% compared to pure PLA [87]. In another previous study, biodegradable biocomposites based on PLA with basalt fibers (BF) or wood fibers (WF) at 7.5 or 15 wt.% were prepared by injection molding. The incorporation of both types of fibers decreased the CTE, which was attributed to the low expansion coefficients of cellulose and basalt. The lowest CTE values were recorded for PLA/15BF, with a 53% decrease compared to pure PLA [88]. PLA-based composites are mainly used in temperature ranges below T_g. The lower CTE in these materials is advantageous for dimensional stability, helping to reduce warping and other shape changes during use, especially under thermomechanical stresses [74].

Table 6. Glass transition temperature and CTE of the PLA and the biocomposites.

Sample	T1 (°C)	α_1 [μm (m·°C)$^{-1}$] 30–50 °C
F0	49.96	95.38
F1	49.22	90.38
F2	49.33	75.53
F3	46.02	85.83
F4	47.94	78.75

Table 6. *Cont.*

Sample	T1 (°C)	α_1 [μm (m·°C)$^{-1}$] 30–50 °C
F5	44.53	77.71
F6	50	76.01
F7	49.65	83.35
F8	46.55	65.04
F9	49.82	76.71
F10	50	81.54
F11	49.31	90.97
F12	48.92	57.72
F13	50	92.04
F14	50	95.33
F15	48.37	81.75
F16	48.15	50.48

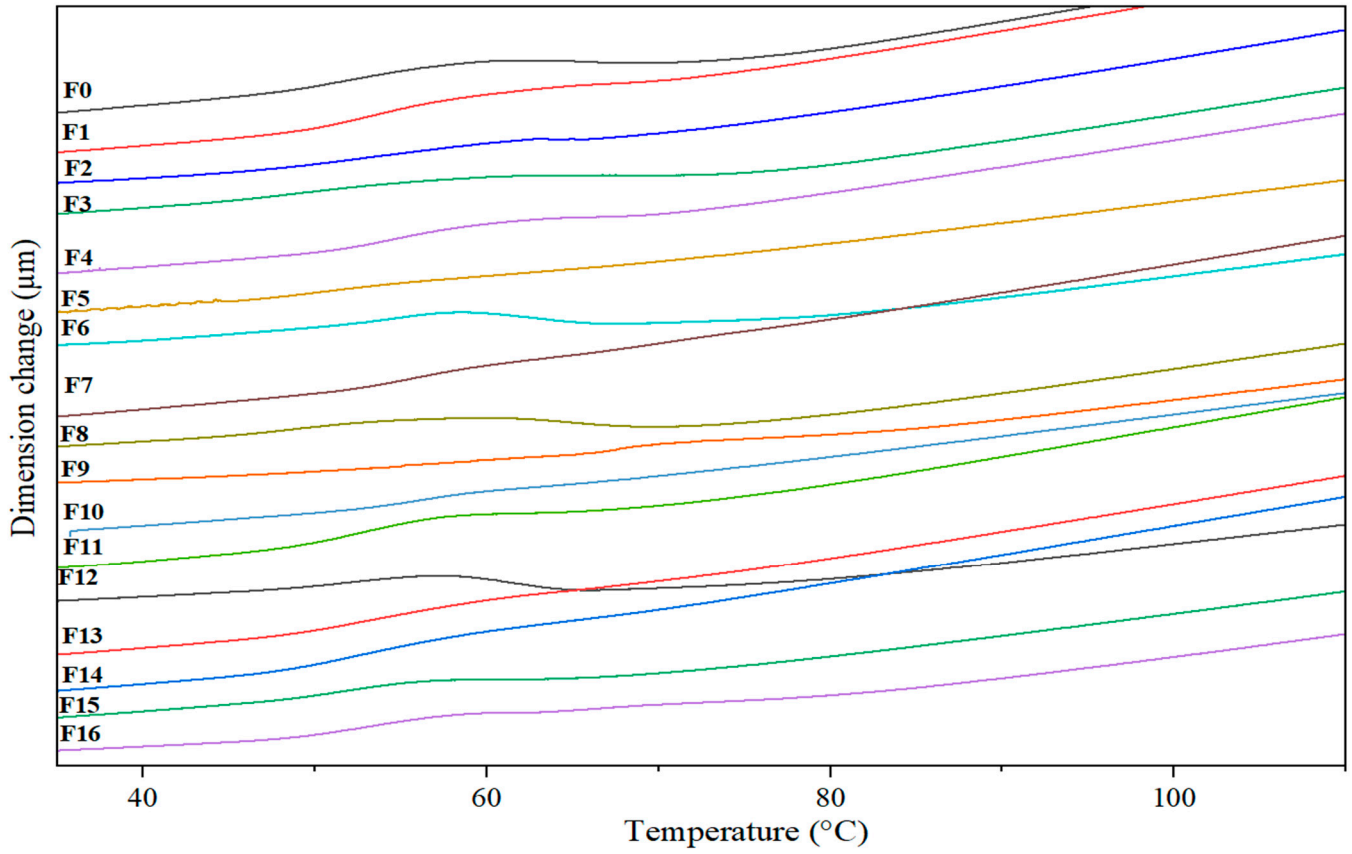


Figure 8. TMA thermograms of the PLA-based composites at different filler contents.

3.2.5. Mechanical Behavior

The results of the flexural tests conducted on the PLA-CPP composites are detailed in Table A1 and illustrated in Figure 9. The flexural strength and modulus show similar trends and increase or decrease depending on the type of treatment used for the incorporated pea pod cellulose. When no PVA compatibilizer was used, the biocomposites reinforced with pea pods treated with 0.5 M OA (CPP1, CPP3) showed higher stiffness and strength compared to those treated with 0.75 M OA (CPP2, CPP4). Conversely, when PVA was included in the formulation, the biocomposites with CPP2 and CPP4 cellulosic reinforcements showed higher modulus and strength. PVA is a water-soluble, nontoxic,

biocompatible, and ductile polymer. Its abundant –OH groups allow the formation of hydrogen bonds with the hydrophilic surfaces of cellulose, which can reduce agglomeration and improve interfacial adhesion [89]. These results are similar to those observed on eco-friendly PLA-MCC biocomposites prepared using two coupling agents: maleic anhydride (MAH) and maleic acid (MA). The incorporation of MAH−MA in the PLA/3 wt.% of MCC composite improved both the tensile strength and the tensile modulus; however, a decrease in elongation at break was observed. Water absorption tests demonstrated that the incorporation of MAH−MA into the PLA/MCC composite led to advantageous water barrier characteristics [72].

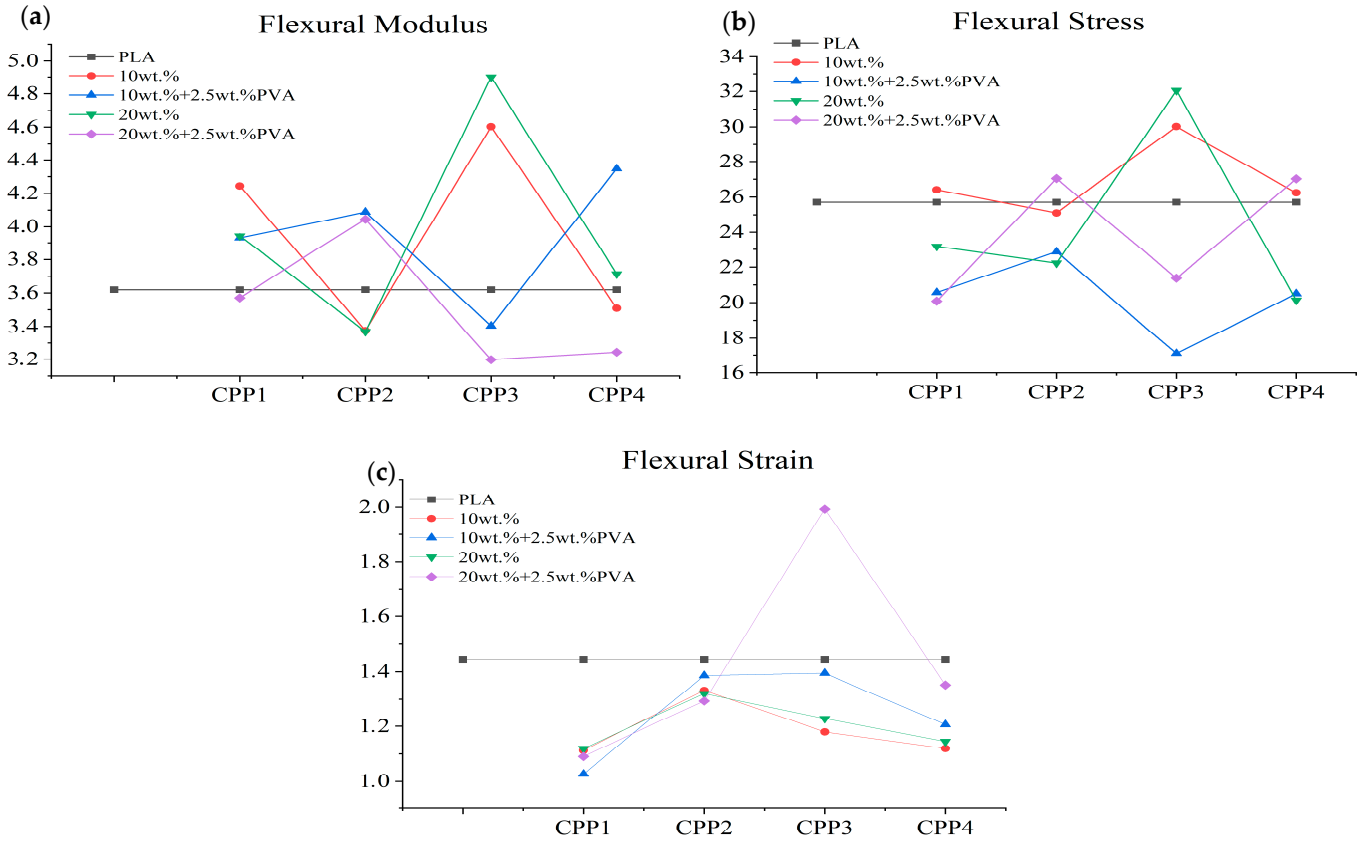


Figure 9. Flexural modulus (**a**), strength (**b**), and strain (**c**) of PLA biocomposites incorporating cellulosic materials obtained through acid and acid-alkaline treatments of pea pod residues.

In general, there were no significant differences in stiffness and strength for the materials with 10 and 20 wt.% cellulosic reinforcements, except for the CPP4. In this case, using only a 10 wt.% reinforcement and PVA resulted in a higher flexural modulus but a lower strength. This can be explained by the improved crystallinity, which leads to the orientation of PLA molecular chains, crystal fragmentation, and slippage during stretching [90].

In addition to the effects of the treatments and the use of compatibilizers, note that the formulations F9 and F10, including pea pods treated with 0.5 M OA and 5 wt.% KOH, without compatibilizer, exhibited the highest flexural modulus and strength among all the formulations studied. Specifically, the average flexural modulus/strength for F9 and F10 increased by 27/17% and 35/24% compared to the PLA matrix, respectively. Suryanegara et al. (2010) studied cellulose-reinforced PLA, obtaining improvements in the modulus from 3.3 GPa to 4.0 GPa and the strength from 50.2 MPa to 60.9 MPa, while the strain at break was reduced from around 7 to 3% [91]. It is also worth mentioning that incorporating 10 wt.% pea pods treated only with 0.5 M OA (F1) increased the average flexural modulus

and strength by 17% and 3%, respectively, compared to the PLA matrix. These results show that friendlier treatments could also result in significant improvements in the mechanical behavior of biocomposites such as the ones studied in this work.

On the other hand, the maximum flexural strain decreased between 10% and 20% for every one of the biocomposites prepared, except for F12. In this case, the strain at failure increased by 37% when a CPP3 cellulosic reinforcement and PVA were used.

3.2.6. Water Absorption

Figure 10 and Table A2 show the percentage of water absorption for PLA and PLA-CPP composites determined after 1 to 21 days of immersion. As expected, the biocomposites exhibited higher water absorption (ranging from 5.8 to 29 after 21 days) compared to neat PLA (3.3% at 21 days). In general, as the cellulosic reinforcement fraction increased, the water absorption also increased. This can be explained by considering the hydrophilic nature of the cellulosic materials, which facilitates the interaction of the biocomposites with water molecules, promoting the formation of hydrogen bonds and the subsequent absorption of water. This was also observed in other previous works. The results obtained in this work align with trends reported in previous studies on cellulose-reinforced PLA biocomposites, where water absorption increases with higher filler content due to the hydrophilic nature of cellulose. For instance, in PLA-based biocomposites reinforced with cellulose derived from durian peel (25 and 35 wt.%), the amount of water absorbed by the composites for 50 days increased with increasing cellulose content. The increase in the cellulose fraction also increased the number of hydroxyl groups (OH) observed [39]. Mahmoud et al. (2022) investigated PLA composites reinforced with microcrystalline cellulose extracted from apricot and walnut shells and showed that composites reached around 5.5% water absorption after ~23 days for samples with 10 wt.% cellulose, while pure PLA absorbed only ~1.5% under the same conditions [92]. These values are still lower than those observed in this study, where water absorption ranged from 5.8% to 29% after 21 days; the higher absorption observed here may be attributed to the combined effect of the specific morphology of pea pod-derived cellulose and the incorporation of PVA. Including PVA in the formulations increases the amount of water absorbed in the samples tested, except for the materials reinforced with pea pods treated with 0.75 M OA. This can be explained by considering that PVA possesses abundant hydroxyl groups along its molecular chains. The incorporation of cellulose fibers into the matrix allows the hydroxyl groups in both cellulose and PVA molecules to form intra- or intermolecular hydrogen bonds [93]. Cellulosic fibers absorb moisture as these hydrogen bonds are broken, enabling the -OH groups to form new hydrogen bonds with water molecules. As a result, the hydrophilic -OH groups contribute to the high-water absorption capacity of cellulosic fibers [94]. Furthermore, differences in immersion temperature (often unspecified) and reinforcement crystallinity may account for variations in the reported values. Overall, the trend of increasing water absorption with cellulose content is consistently observed across studies.

Note also that, for the biocomposites incorporating pea pods treated with 0.75 M OA, the formulations F5 and F7 with 10 wt.% reinforcement have a higher absorption compared to those in which 20 wt.% cellulose was used. This may be due to water penetrating the amorphous phase and catalyzing the hydrolytic degradation of the PLA chains. However, it also depends on the degree of crystallinity, as a high degree of crystallinity limits the hydration of the ordered chains [95].

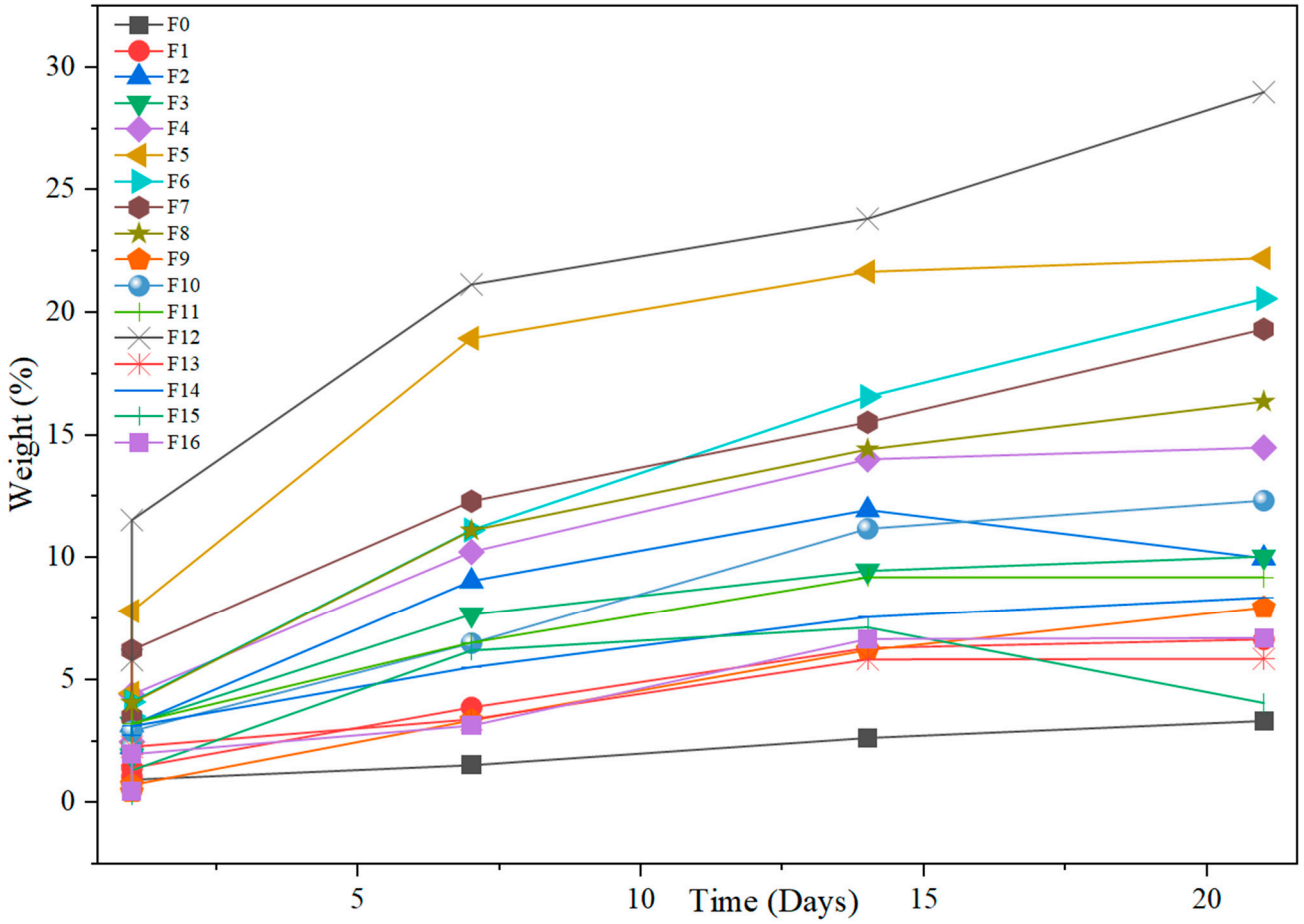


Figure 10. Effect of cellulosic reinforcement content and time on water absorption.

PLA degradation occurs at a faster pace when the temperature is higher than its glass transition temperature (T_g~50–60 °C). However, it is worth mentioning that water absorption also determines the hydrolytic degradation of PLA and its composites [96]. In this work, all the biocomposite samples showed degradation from the seventh day on, except for pure PLA. PLA degrades by simple hydrolysis, which depends on moisture content, molecular weight, crystallinity, molar mass, temperature, and water absorption [94]. As shown in Figure 11, after 21 days, the biocomposite samples exhibited a very porous, fragile structure and typically lost integrity during handling. For that reason, the test could not continue beyond this point.

A visual inspection suggests that the formulation has a significant influence on the presence and distribution of cracks and voids. For instance, the control sample F0 (pure PLA) exhibits extensive cracking and void formation (black arrows), which is consistent with the lack of reinforcement. Sample F5, containing 10% cellulose treated with 0.75 M oxalic acid but without a compatibilizer, shows numerous voids and irregular fiber dispersion, indicating poor interfacial adhesion between fiber and matrix. In contrast, sample F7 (10% cellulose treated with 0.75 M oxalic acid and 2.5% PVA compatibilizer) displays the most favorable morphology: the fibers (red arrows) appear well dispersed and embedded in the PLA matrix, with minimal cracking or voids. This suggests a synergistic effect between the fiber surface treatment and the compatibilizer, resulting in improved fiber–matrix interaction. Other formulations, such as F12 and F14, which include more intense treatments (oxalic acid + KOH) and/or higher fiber content (20%), also benefit from improved morphology compared to F0 and F5 but still exhibit slightly more de-

fects than F7. This could be due to either the increased fiber loading or the less optimal interfacial compatibility.

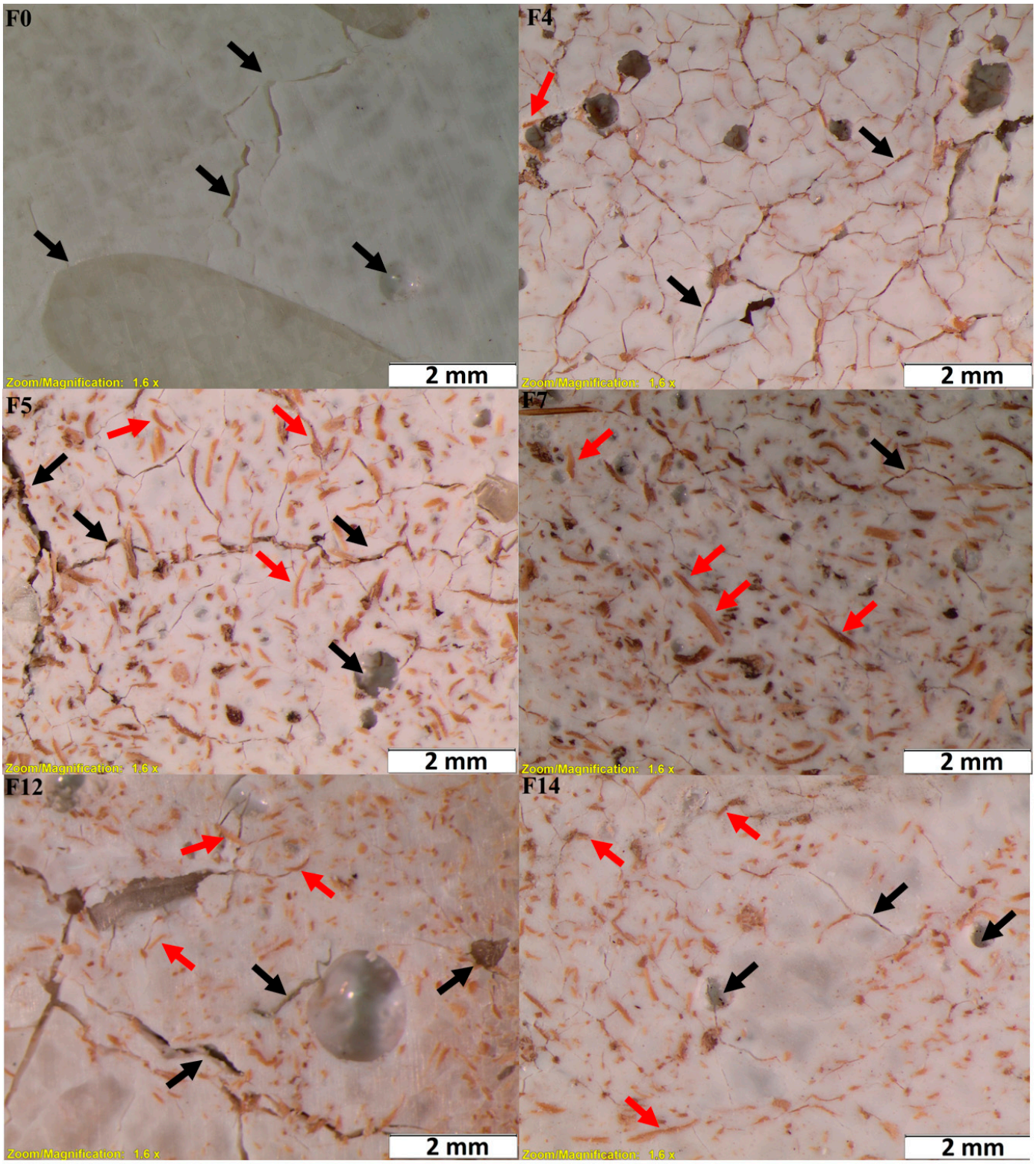


Figure 11. Macrographs of PLA and PLA composite formulations F0, F4, F5, F7, F12, and F14 after 21 days. Black arrows: fractures or voids. Red arrows: cellulose fibers.

While the increase in water absorption observed in the biocomposites may limit their use in moisture-sensitive applications (e.g., structural components or long-term

food packaging), it could be acceptable or even beneficial in short-lifetime applications, such as agricultural mulch films, compostable trays, or disposable packaging, where biodegradability is desired. Moreover, although no surface modification of the cellulose was performed in this study, several works report that chemical treatments such as acetylation, silanization, or grafting with hydrophobic groups can significantly reduce water absorption by lowering the availability of surface hydroxyl groups on cellulose fibers [94,97,98]. These surface modification strategies are promising and will be considered in future work to improve the moisture resistance of these biocomposites and broaden their application range.

4. Conclusions

The use of agroindustrial residues to obtain valuable cellulosic materials constitutes an alternative to mitigate the environmental problems derived from their improper disposal. If these cellulosic materials can be conveniently incorporated as reinforcements for high-performance biocomposites, it is also possible to contribute to reducing the negative impacts of conventional plastics. In this work, we demonstrated that it is feasible to devise high-yield chemical treatments to obtain cellulose from abundant, widely available, inexpensive lignocellulosic residues such as pea pod husks. These treatments offer an opportunity for the valorization of the residues and can be based on the use of low-concentration organic acids, such as 0.5 or 0.75 M OA. This treatment allows us to obtain moderately hydrophilic cellulose with relatively high degradation temperatures (352 or 341 °C). This cellulose can be well dispersed in biodegradable bio-based PLA matrices by extrusion and easily formed by compression molding. The resulting biocomposite specimens are moderately crystalline (29–36%), have glass transition temperatures similar to that of PLA (51–55 °C), and exhibit high degradation temperatures (353–339 °C). They also show higher flexural stiffness (up to 17%), similar strength, and flexural strain at break compared to the pure PLA matrix.

The amount of water absorbed at 50 °C changes significantly (up to 234% of the initial dry weight) depending on the concentration of the oxalic acid, providing opportunities to tailor the composite degradation. On the other hand, if the OA is combined with an alkaline 5% w/v KOH treatment, the cellulose yields are around 64%, the crystallinity reaches values around 92%, while the degradation temperature decreases slightly (T_{max} 328 °C). The biocomposites incorporating these celluloses show T_g, χ_c, and water absorption similar to those obtained with the pea pods treated only with OA. The advantage of these materials is in the mechanical performance, since the flexural modulus and strength can increase up to 35% and 25%, reaching values up to 4.9 GPa and 32.1 MPa, respectively. These values are similar to those obtained using cellulosic reinforcements derived from treatments that include more potentially harmful chemicals. Therefore, the results obtained are encouraging and provide new perspectives for the use of friendlier treatments to obtain moderately crystalline cellulose that can impart good mechanical performance and tailorable degradation to biocomposites.

The incorporation of cellulose from pea pod waste into a PLA matrix improves mechanical strength and water absorption, demonstrating its potential as a sustainable alternative to conventional plastics. These composites are particularly well-suited for biodegradable packaging, agricultural films, and short-life disposable items, where renewable origin, reinforcement, hydrophilicity, and biodegradability are essential. The valorization of agro-industrial waste further highlights the environmental and practical significance of these materials.

Author Contributions: D.N.-B., V.H.G. and P.I.P. contributed to the study conceptualization and design. Material preparation, data collection, analysis, and first draft preparation were performed by D.N.-B., S.G. and J.T. contributed to the experimental testing. V.H.G. managed the project and

contributed to formal analysis. A.D. contributed to formal analysis and validation. All authors have read and agreed to the published version of the manuscript.

Funding: This work was supported by the Escuela Politécnica Nacional, from Quito, Ecuador. No grant was received during the preparation of this manuscript.

Institutional Review Board Statement: Not applicable.

Informed Consent Statement: Not applicable.

Data Availability Statement: The original contributions presented in this study are included in the article. Further inquiries can be directed to the corresponding author.

Acknowledgments: The authors gratefully acknowledge the Escuela Politécnica Nacional and its Department of Chemical Engineering, Center for Applied Polymer Research, and Laboratory for Stress Analysis and Vibration, for their collaboration in performing the XRD, FTIR, and mechanical characterizations.

Conflicts of Interest: The authors declare no conflicts of interest.

Appendix A

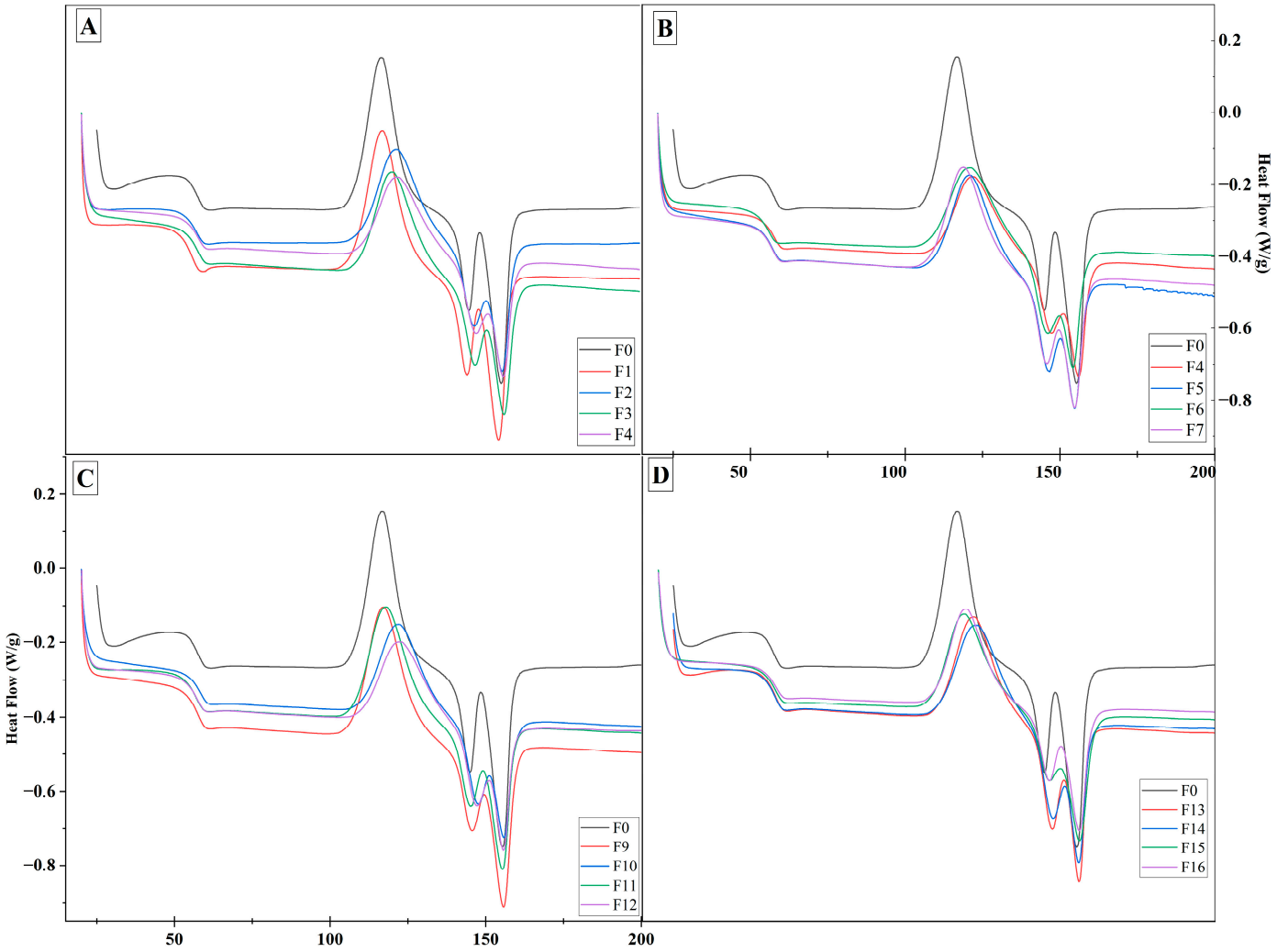


Figure A1. DSC thermograms of the second heating for PLA and PLA-based composites with different cellulosic content. (**A**) CPP1 treatment; (**B**) CPP2 treatment; (**C**) CPP3 treatment; (**D**) CPP4 treatment.

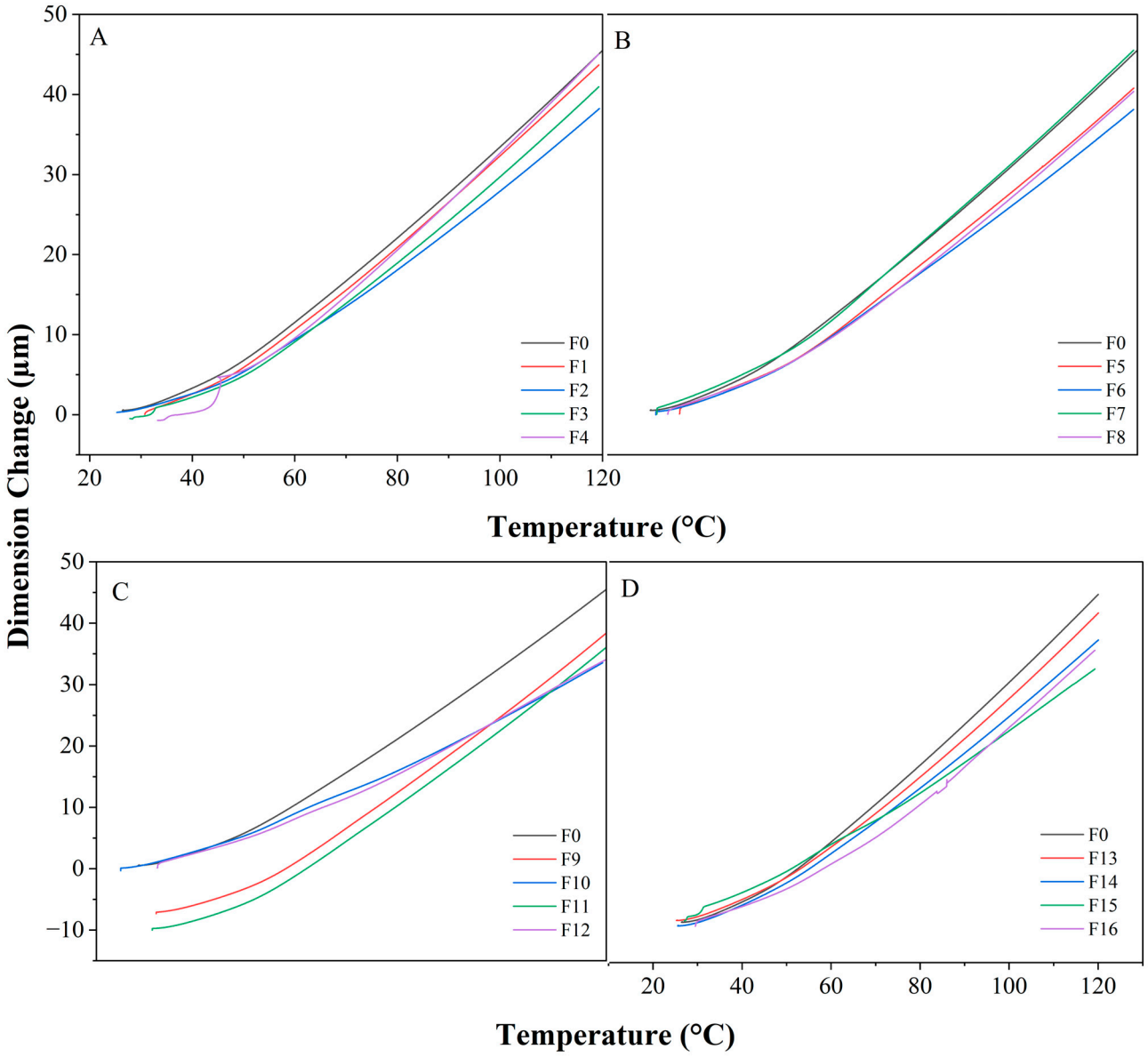


Figure A2. TMA thermograms of the second heating for PLA-based composites at different filler content. (**A**) CPP1 treatment; (**B**) CPP2 treatment; (**C**) CPP3 treatment; (**D**) CPP4 treatment.

Table A1. Mechanical properties of neat PLA and its biocomposites with cellulosic reinforcements.

Samples	Flexural Modulus (GPa)	Flexural Strength (MPa)	Flexural Strain (%)
F0	3.620 ± 0.102	25.710 ± 3.973	1.445 ± 0.093
F1	4.244 ± 0.249	26.407 ± 3.179	1.112 ± 0.057
F2	3.942 ± 0.074	23.168 ± 2.536	1.119 ± 0.046
F3	3.931 ± 0.404	20.576 ± 2.297	1.027 ± 0.117
F4	3.571 ± 0.176	20.086 ± 1.832	1.091 ± 0.119
F5	3.375 ± 0.417	25.104 ± 3.583	1.332 ± 0.131
F6	3.369 ± 0.189	22.225 ± 1.609	1.320 ± 0.059
F7	4.088 ± 0.201	22.863 ± 2.820	1.386 ± 0.224
F8	4.045 ± 0.322	27.036 ± 0.867	1.293 ± 0.096

Table A1. *Cont.*

Samples	Flexural Modulus (GPa)	Flexural Strength (MPa)	Flexural Strain (%)
F9	4.603 ± 0.750	30.018 ± 1.085	1.179 ± 0.150
F10	4.900 ± 0.215	32.051 ± 2.997	1.228 ± 0.085
F11	3.403 ± 0.154	17.108 ± 1.574	1.395 ± 0.316
F12	3.197 ± 0.568	21.371 ± 0.387	1.993 ± 0.499
F13	3.509 ± 0.143	26.235 ± 0.733	1.119 ± 0.040
F14	3.713 ± 0.216	20.137 ± 1.086	1.144 ± 0.253
F15	3.619 ± 0.127	19.890 ± 2.474	1.131 ± 0.145
F16	3.700 ± 0.234	18.969 ± 2.084	1.117 ± 0.060

Table A2. Water absorption of neat PLA and composites reinforced with cellulose.

	Water Absorption (%)				
Time (Days)	**1**	**2**	**7**	**14**	**21**
F0	0.708	0.934	1.522	2.631	3.319
F1	1.062	1.411	3.875	6.291	6.637
F2	2.271	3.166	9.040	11.944	9.975
F3	1.908	3.197	7.665	9.457	10.050
F4	2.472	4.395	10.235	14.016	14.494
F5	4.453	7.806	18.951	21.669	22.222
F6	3.505	4.091	11.132	16.568	20.570
F7	3.486	6.203	12.306	15.526	19.326
F8	2.320	4.061	11.114	14.417	16.368
F9	0.442	0.724	3.340	6.207	7.953
F10	2.237	2.907	6.483	11.178	12.331
F11	2.211	3.225	6.515	9.196	9.196
F12	5.795	11.534	21.149	23.833	28.992
F13	1.955	2.273	3.388	5.822	5.844
F14	2.717	3.103	5.509	7.560	8.359
F15	0.285	1.318	6.185	7.130	4.048
F16	0.459	1.973	3.128	6.656	6.698

Table A3. Mechanical performance of PLA and composites reinforced with cellulose.

Sample	Relation	Flexural Modulus (GPa)	Flexural Strength (MPa)	Flexural Strain (%)	Results	References
PLA	100	3	8.4	--	The flexural modulus and strength increase by 25% and 80%, respectively, with 20% of MFC. Flexural strength increases by 130% with 1% CNC. At 5% CNC, the flexural modulus increases to 175%	[10]
PLA-cellulose microfibers (MFC)	80:20	3.8	16.5	--		
PLA-MFC-cellulose nanocrystals (CNC)	80:19:1 80:15:5	5.3 5.7	19.2 26.5	--		

Table A3. *Cont.*

Sample	Relation	Flexural Modulus (GPa)	Flexural Strength (MPa)	Flexural Strain (%)	Results	References
PLA	100	1.17	15.24	40.30	At 1% CNF-Ac into PLA films, the strain increased by more than 60 percent. CNF-Ac to 3%, the tensile strength and tensile modulus increase.	[99]
PLA/acetylated cellulose nanofiber (CNF-Ac)-1	1% CNF-Ac	1.13	16.70	64.77		
PLA/CNF-Ac-3	3% CNF-Ac	1.20	33.06	188.86		
PLA/microcrystalline cellulose (MCC)-3	3% MCC	1.19	15.88	38.47		
PLA	100		14.72	10.32	At 1 wt% NFC, the tensile strain increases to 87.9% compared with PLA. When NFC is at 5 wt%, tensile strength reaches a 98.8% boost.	[90]
PLA/nanofibrillated cellulose (NFC)-3wt%	3 wt% NFC		27.08	17.95		
PLA/NFC-5wt%	5 wt% NFC		29.26	18.67		
PLA/NFC-10wt%	10 wt% NFC		26.30	15.71		
PLA	100	3.3	57.7	6.8	20 wt% of MFC improved the modulus of amorphous PLA from 3.3 GPa to 5.2 GPa and the tensile strength.	[100]
PLA/microfibrillated cellulose (MFC) 3wt%	3 wt% MFC	3.8	61.4	2.7		
PLA/MFC 5wt%	5 wt% MFC	3.9	63.4	2.5		
PLA/MFC 10wt%	10 wt% MFC	4.5	65.4	2.2		
PLA/MFC 20wt%	20 wt% MFC	5.2	70.2	1.9		

References

1. Samir, A.; Ashour, F.H.; Hakim, A.A.A.; Bassyouni, M. Recent Advances in Biodegradable Polymers for Sustainable Applications. *Npj Mater. Degrad.* **2022**, *6*, 68. [CrossRef]
2. Rosenboom, J.-G.G.; Langer, R.; Traverso, G. Bioplastics for a Circular Economy. *Nat. Rev. Mater.* **2022**, *7*, 117–137. [CrossRef]
3. Negrete-Bolagay, D.; Guerrero, V.H. Opportunities and Challenges in the Application of Bioplastics: Perspectives from Formulation, Processing, and Performance. *Polymers* **2024**, *16*, 2561. [CrossRef]
4. Galera Manzano, L.M.; Ruz Cruz, M.Á.; Moo Tun, N.M.; Valadez González, A.; Mina Hernandez, J.H. Effect of Cellulose and Cellulose Nanocrystal Contents on the Biodegradation, under Composting Conditions, of Hierarchical PLA Biocomposites. *Polymers* **2021**, *13*, 1855. [CrossRef]
5. Chavhan, G.R.; Wankhade, L.N. Improvement of the Mechanical Properties of Hybrid Composites Prepared by Fibers, Fiber-Metals, and Nano-Filler Particles—A Review. *Mater. Today Proc.* **2020**, *27*, 72–82. [CrossRef]
6. Vigneshwaran, S.; Sundarakannan, R.; John, K.M.; Joel Johnson, R.D.; Prasath, K.A.; Ajith, S.; Arumugaprabu, V.; Uthayakumar, M. Recent Advancement in the Natural Fiber Polymer Composites: A Comprehensive Review. *J. Clean. Prod.* **2020**, *277*, 124109. [CrossRef]
7. Rasheed, M.; Jawaid, M.; Parveez, B.; Zuriyati, A.; Khan, A. *Morphological, Chemical and Thermal Analysis of Cellulose Nanocrystals Extracted from Bamboo Fibre*; Elsevier: Amsterdam, The Netherlands, 2020; Volume 160. [CrossRef]
8. Thakur, V.K.; Thakur, M.K. Processing and Characterization of Natural Cellulose Fibers/Thermoset Polymer Composites. *Carbohydr. Polym.* **2014**, *109*, 102–117. [CrossRef]
9. Sharma, A.; Thakur, M.; Bhattacharya, M.; Mandal, T.; Goswami, S. Commercial Application of Cellulose Nano-Composites—A Review. *Biotechnol. Rep.* **2019**, *21*, e00316. [CrossRef] [PubMed]
10. Ruz-Cruz, M.A.A.; Herrera-Franco, P.J.J.; Flores-Johnson, E.A.A.; Moreno-Chulim, M.V.V.; Galera-Manzano, L.M.M.; Valadez-González, A. Thermal and Mechanical Properties of PLA-Based Multiscale Cellulosic Biocomposites. *J. Mater. Res. Technol.* **2022**, *18*, 485–495. [CrossRef]
11. Ilyas, R.A.; Sapuan, S.M.; Sabaruddin, F.A.; Atikah, M.S.N.; Ibrahim, R.; Asyraf, M.R.M.; Huzaifah, M.R.M.; Saifulazry, S.O.A.; Ainun, Z.M.A. Reuse and Recycle of Biobased Packaging Products. In *Bio-Based Packaging: Material, Environmental and Economic Aspects*; Wiley: Hoboken, NJ, USA, 2021; pp. 413–426. [CrossRef]

12. Campaña, O.; Guerrero; Hugo, V. Caracterización Mecánica y Térmica de Ácido Poliláctico (PLA) Reforzado Con Polvo de Bambú (PB). *Rev. Politec.* **2018**, *42*, 8.
13. Safdari, F.; Bagheriasl, D.; Carreau, P.J.; Heuzey, M.C.; Kamal, M.R. Rheological, Mechanical, and Thermal Properties of Polylactide/Cellulose Nanofiber Biocomposites. *Polym. Compos.* **2018**, *39*, 1752–1762. [CrossRef]
14. Jiang, Y.; Liu, X.; Yang, S.; Song, X.; Wang, S. Combining Organosolv Pretreatment with Mechanical Grinding of Sugarcane Bagasse for the Preparation of Nanofibrillated Cellulose in a Novel Green Approach. *Bioresources* **2018**, *14*, 313–335. [CrossRef]
15. Wijekoon, N.K.; Appuhamillage, G.A.; Dassanayake, R.S.; Liyanage, R.N.; Mapage, D.; Wijenayake, A.; Lokuge, E.L.; Rajapaksha, S.M.; Abeygunawardane, G.A.; Senarath, N.D.D.D. Facile Fabrication of 3D-Printed Cellulosic Fiber/Polylactic Acid Composites as Low-Cost and Sustainable Acoustic Panels. *Sustain. Chem. Environ.* **2024**, *8*, 100–168. [CrossRef]
16. Tarrés, Q.; Espinosa, E.; Domínguez-Robles, J.; Rodríguez, A.; Mutjé, P.; Delgado-Aguilar, M. The Suitability of Banana Leaf Residue as Raw Material for the Production of High Lignin Content Micro/Nano Fibers: From Residue to Value-Added Products. *Ind. Crops Prod.* **2017**, *99*, 27–33. [CrossRef]
17. Espinosa, E.; Sánchez, R.; Otero, R.; Domínguez-Robles, J.; Rodríguez, A. A Comparative Study of the Suitability of Different Cereal Straws for Lignocellulose Nanofibers Isolation. *Int. J. Biol. Macromol.* **2017**, *103*, 990–999. [CrossRef]
18. Lecoublet, M.; Ragoubi, M.; Leblanc, N.; Koubaa, A. Sustainable 3D-Printed Cellulose-Based Biocomposites and Bio-Nano-Composites: Analysis of Dielectric Performances. *Ind. Crops Prod.* **2024**, *221*, 119–332. [CrossRef]
19. Bahrami, P.; Morsali, P.; Abbasi, D.; Hemmati, F.; Mohammadi-Roshandeh, J. Environmentally-Friendly Solvent Pulping and Grafting Strategies for Better Foamability of Poly(Lactic Acid)/Agricultural Waste Biocomposites. *J. Reinf. Plast. Compos.* **2024**, *75*, 1. [CrossRef]
20. Jiang, Y.; Liu, X.; Yang, Q.; Song, X.; Qin, C.; Wang, S.; Li, K. Effects of Residual Lignin on Mechanical Defibrillation Process of Cellulosic Fiber for Producing Lignocellulose Nanofibrils. *Cellulose* **2018**, *25*, 6479–6494. [CrossRef]
21. Chihaoui, B.; Tarrés, Q.; Delgado-Aguilar, M.; Mutjé, P.; Boufi, S. Lignin-Containing Cellulose Fibrils as Reinforcement of Plasticized PLA Biocomposites Produced by Melt Processing Using PEG as a Carrier. *Ind. Crops Prod.* **2022**, *175*, 114–287. [CrossRef]
22. Linares, M.G.; Delgado Aguilar, M.; Tarrés, J.; Aguado, R.; Pereira, M.; Valerio, O. Impact of Lignocellulosic Nanofiber Source on the Performance of Polylactic Acid. *J. Appl. Polym. Sci.* **2024**, *141*, e56088. [CrossRef]
23. Vanderfleet, O.M.; Cranston, E.D. Production Routes to Tailor the Performance of Cellulose Nanocrystals. *Nat. Rev. Mater.* **2020**, *6*, 124–144. [CrossRef]
24. Choi, H.Y.; Lee, J.S. Effects of Surface Treatment of Ramie Fibers in a Ramie/Poly(Lactic Acid) Composite. *Fibers Polym.* **2012**, *13*, 217–223. [CrossRef]
25. Verma, N.; Mukesh, C.B.; Vivek, K. Pea Peel Waste: A Lignocellulosic Waste and Its Utility in Cellulase Production. *Bioresources* **2011**, *6*, 1505–1519. [CrossRef]
26. Nimbalkar, P.R.; Khedkar, M.A.; Chavan, P.V.; Bankar, S.B. Biobutanol Production Using Pea Pod Waste as Substrate: Impact of Drying on Saccharification and Fermentation. *Renew. Energy* **2018**, *117*, 520–529. [CrossRef]
27. Fatima, R.; Fatima, F.; Altemimi, A.B.; Bashir, N.; Sipra, H.M.; Hassan, S.A.; Mujahid, W.; Shehzad, A.; Abdi, G.; Aadil, R.M. Bridging Sustainability and Industry through Resourceful Utilization of Pea Pods- A Focus on Diverse Industrial Applications. *Food Chem.* **2024**, *23*, 101–518. [CrossRef]
28. Abolore, R.S.; Jaiswal, S.; Jaiswal, A.K. Green and Sustainable Pretreatment Methods for Cellulose Extraction from Lignocellulosic Biomass and Its Applications: A Review. *Carbohydr. Polym. Technol. Appl.* **2024**, *7*, 100396. [CrossRef]
29. Herrera-Barrios, A.; Puello-Mendez, J.; Pasqualino, J.C.; Lambis-Miranda, H.A. Agro-Industrial Waste from Cocoa Pod Husk (*Theobroma cacao* L.), as a Potential Raw Material for Preparation of Cellulose Nanocrystals. *Chem. Eng. Trans.* **2022**, *92*, 205–210. [CrossRef]
30. *ASTM E872-82(2019)*; Test Method for Volatile Matter in the Analysis of Particulate Wood Fuels. ASTM International: West Conshohocken, PA, USA, 2019. [CrossRef]
31. *ASTM D1106-21*; Test Method for Acid-Insoluble Lignin in Wood. ASTM International: West Conshohocken, PA, USA, 2021. [CrossRef]
32. *ASTM D1107-21*; Test Method for Ethanol-Toluene Solubility of Wood. ASTM International: West Conshohocken, PA, USA, 2021. [CrossRef]
33. *ASTM D1109-21*; Test Method for 1 % Sodium Hydroxide Solubility of Wood. ASTM International: West Conshohocken, PA, USA, 2021. [CrossRef]
34. MDI Materials Data. *JADE Pro*; MDI Materials Data: Livermore, CA, USA, 2025.
35. Tejedor, J.; Cevallos, P.D.; Coro, E.S.; Pontón, P.I.; Guamán, M.; Guerrero, V.H. Effects of Annealing on the Mechanical, Thermal, and Physical Properties of 3D-Printed PLA Aged in Salt Water. *Mech. Adv. Mater. Struct.* **2024**, *32*, 2307–2321. [CrossRef]
36. Pontón, P.I.; Prisco, L.P.; Marinkovic, B.A. Effects of Low Contents of $A_2M_3O_{12}$ Submicronic Thermomiotic-like Fillers on Thermal Expansion and Mechanical Properties of HDPE-Based Composites. *Polym. Compos.* **2018**, *39*, 1821–1833. [CrossRef]

37. *ASTM D790-17*; Test Methods for Flexural Properties of Unreinforced and Reinforced Plastics and Electrical Insulating Materials. ASTM International: West Conshohocken, PA, USA, 2017. [CrossRef]
38. *ASTM D792-20*; Test Methods for Density and Specific Gravity (Relative Density) of Plastics by Displacement. ASTM International: West Conshohocken, PA, USA, 2020. [CrossRef]
39. Penjumras, P.; Rahman, R.A.; Talib, R.A.; Abdan, K. Mechanical Properties and Water Absorption Behaviour of Durian Rind Cellulose Reinforced Poly(Lactic Acid) Biocomposites. *Int. J. Adv. Sci. Eng. Inf. Technol.* **2015**, *5*, 343–349. [CrossRef]
40. Li, D.; Henschen, J.; Ek, M. Esterification and Hydrolysis of Cellulose Using Oxalic Acid Dihydrate in a Solvent-Free Reaction Suitable for Preparation of Surface-Functionalised Cellulose Nanocrystals with High Yield. *Green. Chem.* **2017**, *19*, 5564–5567. [CrossRef]
41. Zambrano-Mite, L.F.; Villasana, Y.; Bejarano, M.L.; Luciani, C.; Niebieskikwiat, D.; Álvarez, W.; Cueva, D.F.; Aguilera-Pesantes, D.; Orejuela-Escobar, L.M. Optimization of Microfibrillated Cellulose Isolation from Cocoa Pod Husk via Mild Oxalic Acid Hydrolysis: A Response Surface Methodology Approach. *Heliyon* **2023**, *9*, e17258. [CrossRef] [PubMed]
42. Cheng, B.; Zhang, X.; Lin, Q.; Xin, F.; Sun, R.; Wang, X.; Ren, J. A New Approach to Recycle Oxalic Acid during Lignocellulose Pretreatment for Xylose Production. *Biotechnol. Biofuels* **2018**, *11*, 324. [CrossRef] [PubMed]
43. Deng, A.; Ren, J.; Wang, W.; Li, H.; Lin, Q.; Yan, Y.; Sun, R.; Liu, G. Production of Xylo-Sugars from Corncob by Oxalic Acid-Assisted Ball Milling and Microwave-Induced Hydrothermal Treatments. *Ind. Crops Prod.* **2016**, *79*, 137–145. [CrossRef]
44. Xu, W.; Grénman, H.; Liu, J.; Kronlund, D.; Li, B.; Backman, P.; Peltonen, J.; Willför, S.; Sundberg, A.; Xu, C. Mild Oxalic-Acid-Catalyzed Hydrolysis as a Novel Approach to Prepare Cellulose Nanocrystals. *ChemNanoMat* **2017**, *3*, 109–119. [CrossRef]
45. Poulose, A.; Parameswaranpillai, J.; George, J.J.; Gopi, J.A.; Krishnasamy, S.; Dominic, C.D.M.; Hameed, N.; Salim, N.V.; Radoor, S.; Sienkiewicz, N. Nanocellulose: A Fundamental Material for Science and Technology Applications. *Molecules* **2022**, *27*, 8032. [CrossRef]
46. Przypis, M.; Wawoczny, A.; Gillner, D. Biomass and Cellulose Dissolution—The Important Issue in Renewable Materials Treatment. *Appl. Sci.* **2023**, *13*, 1055. [CrossRef]
47. Luo, J.; Huang, K.; Xu, Y.; Fan, Y. A Comparative Study of Lignocellulosic Nanofibrils Isolated from Celery Using Oxalic Acid Hydrolysis Followed by Sonication and Mechanical Fibrillation. *Cellulose* **2019**, *26*, 5237–5246. [CrossRef]
48. Romruen, O.; Karbowiak, T.; Tongdeesoontorn, W.; Shiekh, K.A.; Rawdkuen, S. Extraction and Characterization of Cellulose from Agricultural By-Products of Chiang Rai Province, Thailand. *Polymers* **2022**, *14*, 1830. [CrossRef]
49. Bastida, G.A.; Schnell, C.N.; Mocchiutti, P.; Solier, Y.N.; Inalbon, M.C.; Zanuttini, M.Á.; Galván, M.V. Effect of Oxalic Acid Concentration and Different Mechanical Pre-Treatments on the Production of Cellulose Micro/Nanofibers. *Nanomaterials* **2022**, *12*, 2908. [CrossRef]
50. Xu, Y.; Wang, J.; Qian, X.; Zuo, L.; Yue, X. Effects of Supplementary Alkali after Alkaline Peroxide on the Properties of Bleached Kraft Pine Fluff. *Bioresources* **2016**, *11*, 336–353. [CrossRef]
51. Kamaruddin, Z.H.; Jumaidin, R.; Ilyas, R.A.; Selamat, M.Z.; Alamjuri, R.H.; Md Yusof, F.A. Influence of Alkali Treatment on the Mechanical, Thermal, Water Absorption, and Biodegradation Properties of *Cymbopogan citratus* Fiber-Reinforced, Thermoplastic Cassava Starch–Palm Wax Composites. *Polymers* **2022**, *14*, 2769. [CrossRef]
52. Gudayu, A.D.; Steuernagel, L.; Meiners, D.; Gideon, R. Effect of Surface Treatment on Moisture Absorption, Thermal, and Mechanical Properties of Sisal Fiber. *J. Ind. Text.* **2022**, *51*, 2853–2873. [CrossRef]
53. Delgado-Orti, C.; Navas-Martos, F.J.; Rodríguez-Liébana, J.A.; La Rubia, M.D.; Jurado-Contreras, S. Development of PLA–Waste Paper Biocomposites with High Cellulose Content. *Polymers* **2024**, *16*, 2000. [CrossRef]
54. Bhiri, F.; Abidi, S.; Bouallegue, A.; Bensidhom, G.; Kallel, F.; Ellouz Chaabouni, S.; Trabelsi, A.B.H. Valorization of Pea By-Products for the Isolation of Cellulosic Micro Bers: Extraction and Physico- Chemical Characterization. *Res. Sq.* **2022**. [CrossRef]
55. Alshahrani, H.; Arun Prakash, V.R. Characterisation of Microcrystalline Cellulose from Waste Green Pea Pod Sheath and Its Sunn Hemp Fibre-Polyester Composite: A Step towards Greener Manufacturing. *Physiol. Plant* **2024**, *176*, e14166. [CrossRef]
56. Salim, M.H.; Abdellaoui, Y.; Ait Benhamou, A.; Ablouh, E.H.; El Achaby, M.; Kassab, Z. Influence of Cellulose Nanocrystals from Pea Pod Waste on Mechanical, Thermal, Biodegradability, and Barrier Properties of Chitosan-Based Films. *Cellulose* **2022**, *29*, 5117–5135. [CrossRef]
57. Mamudu, U.; Kabyshev, A.; Bekmyrza, K.; Kuterbekov, K.A.; Baratova, A.; Omeiza, L.A.; Lim, R.C. Extraction, Preparation and Characterization of Nanocrystalline Cellulose from Lignocellulosic Simpor Leaf Residue. *Molecules* **2025**, *30*, 1622. [CrossRef] [PubMed]
58. Poletto, M.; Pistor, V.J.A. Structural Characteristics and Thermal Properties of Native Cellulose. In *Cellulose—Fundamental Aspects*; InTech: Vienna, Austria, 2013. [CrossRef]
59. Trilokesh, C.; Uppuluri, K.B. Isolation and Characterization of Cellulose Nanocrystals from Jackfruit Peel. *Sci. Rep.* **2019**, *9*, 16709. [CrossRef]
60. Kulandaivel, N.; Muralikannan, R.; KalyanaSundaram, S. Extraction and Characterization of Novel Natural Cellulosic Fibers from Pigeon Pea Plant. *J. Nat. Fibers* **2020**, *17*, 769–779. [CrossRef]

61. Bhiri, F.; Abidi, S.; Bouallegue, A.; Bensidhom, G.; Kallel, F. A Renewable Cellulose Source: Isolation and Characterization of Cellulose Microfibers from Pea Pod Waste. In *Recent Advances in Environmental Science from the Euro-Mediterranean and Surrounding Regions*; Springer: Cham, Switzerland, 2024; pp. 41–44. [CrossRef]
62. Mathew, A.P.; Oksman, K.; Sain, M. Mechanical Properties of Biodegradable Composites from Poly Lactic Acid (PLA) and Microcrystalline Cellulose (MCC). *J. Appl. Polym. Sci.* **2005**, *97*, 2014–2025. [CrossRef]
63. Mostafa, N.A.; Farag, A.A.; Abo-dief, H.M.; Tayeb, A.M. Production of Biodegradable Plastic from Agricultural Wastes. *Arab. J. Chem.* **2018**, *11*, 546–553. [CrossRef]
64. Kabekkodu, S.N.; Dosen, A.; Blanton, T.N. PDF-5+: A Comprehensive Powder Diffraction File^{TM} for Materials Characterization. *Powder Diffr.* **2024**, *39*, 47–59. [CrossRef]
65. Mostafa, S.; Bockisch, F.J. Mechanical Properties of Some Bioplastics Under Different Soil Types for Use as a Biodegradable Drip Tubes. *Agric. Eng. Int. CIGR J.* **2010**, *12*, 1–16.
66. Kassab, Z.; Abdellaoui, Y.; Salim, M.H.; El Achaby, M. Cellulosic Materials from Pea (*Pisum sativum*) and Broad Beans (*Vicia faba*) Pods Agro-Industrial Residues. *Mater. Lett.* **2020**, *280*, 128539. [CrossRef]
67. Singh, S.; Bhardwaj, S.; Meda, R.S.; Verma, C.; Chhajed, M.; Ghosh, K.; Maji, P.K. Insights into Thermal Degradation Kinetics and Liquid Crystalline Behavior of Cellulose Nanocrystals from the Waste of *Cajanus cajan* (Pigeon Pea). *Int. J. Biol. Macromol.* **2023**, *242*, 124507. [CrossRef]
68. Lapuz, A.R.; Tsuchikawa, S.; Inagaki, T.; Ma, T.; Migo, V. Production of Nanocellulose Film from Abaca Fibers. *Crystals* **2022**, *12*, 601. [CrossRef]
69. Al-Awa, Z.F.A.; Sangor, F.I.M.S.; Babili, S.B.; Saud, A.; Saleem, H.; Zaidi, S.J. Effect of Leaf Powdering Technique on the Characteristics of Date Palm-Derived Cellulose. *ACS Omega* **2023**, *8*, 18930–18939. [CrossRef]
70. Zhang, X.; Wang, F.; Keer, L.M. Influence of Surface Modification on the Microstructure and Thermo-Mechanical Properties of Bamboo Fibers. *Materials* **2015**, *8*, 6597–6608. [CrossRef]
71. Cichosz, S.; Masek, A.; Wolski, K.; Zaborski, M. Universal Approach of Cellulose Fibres Chemical Modification Result Analysis via Commonly Used Techniques. *Polym. Bull.* **2019**, *76*, 2147–2162. [CrossRef]
72. Gorgun, E.; Ali, A.; Islam, M.S. Biocomposites of Poly(Lactic Acid) and Microcrystalline Cellulose: Influence of the Coupling Agent on Thermomechanical and Absorption Characteristics. *ACS Omega* **2024**, *9*, 11523–11533. [CrossRef]
73. Raisipour-Shirazi, A.; Ahmadi, Z.; Garmabi, H. Polylactic Acid Nanocomposites Toughened with Nanofibrillated Cellulose: Microstructure, Thermal, and Mechanical Properties. *Iran. Polym. J.* **2018**, *27*, 785–794. [CrossRef]
74. Espinach, F.X.; Boufi, S.; Delgado-Aguilar, M.; Julián, F.; Mutjé, P.; Méndez, J.A. Composites from Poly(Lactic Acid) and Bleached Chemical Fibres: Thermal Properties. *Compos. B Eng.* **2018**, *134*, 169–176. [CrossRef]
75. Phiri, R.; Rangappa, S.M.; Siengchin, S. Sugarcane Bagasse for Sustainable Development of Thermoset Biocomposites. *J. Polym. Res.* **2024**, *31*, 317–320. [CrossRef]
76. Shojaeiarani, J.; Bajwa, D.S.; Stark, N.M. Green Esterification: A New Approach to Improve Thermal and Mechanical Properties of Poly(Lactic Acid) Composites Reinforced by Cellulose Nanocrystals. *J. Appl. Polym. Sci.* **2018**, *135*, 46468. [CrossRef]
77. Wu, H.; Liu, X.; Hua, X.; Zhang, J. Thermal-Oxidation Degradation of Polylactic Acid/Cellulose Nanocrystal Composites: Effects of Surface Chemistry. *Ind Crops Prod* **2023**, 202. [CrossRef]
78. Tan, L.; Liu, L.; Liu, C.; Wang, W. Improvement in the Performance of the Polylactic Acid Composites by Using Deep Eutectic Solvent Treated Pulp Fiber. *J. Renew. Mater.* **2021**, *9*, 1897–1911. [CrossRef]
79. Bhiogade, A.; Kannan, M. Studies on Thermal and Degradation Kinetics of Cellulose Micro/Nanoparticle Filled Polylactic Acid (PLA) Based Nanocomposites. *Polym. Polym. Compos.* **2021**, *29* (Suppl. 9), S85–S98. [CrossRef]
80. Frone, A.N.; Panaitescu, D.M.; Chiulan, I.; Nicolae, C.A.; Vuluga, Z.; Vitelaru, C.; Damian, C.M. The Effect of Cellulose Nanofibers on the Crystallinity and Nanostructure of Poly(Lactic Acid) Composites. *J. Mater. Sci.* **2016**, *51*, 9771–9791. [CrossRef]
81. Fiore, V.; Botta, L.; Scaffaro, R.; Valenza, A.; Pirrotta, A. PLA Based Biocomposites Reinforced with *Arundo donax* Fillers. *Compos. Sci. Technol.* **2014**, *105*, 110–117. [CrossRef]
82. Wach, R.A.; Wolszczak, P.; Adamus-Wlodarczyk, A. Enhancement of Mechanical Properties of FDM-PLA Parts via Thermal Annealing. *Macromol. Mater. Eng.* **2018**, *303*, 1800169. [CrossRef]
83. Rahman, M.M.; Afrin, S.; Haque, P.; Islam, M.M.; Islam, M.S.; Gafur, M.A. Preparation and Characterization of Jute Cellulose Crystals-Reinforced Poly(l-Lactic Acid) Biocomposite for Biomedical Applications. *Int. J. Chem. Eng.* **2014**, *2014*, 842147. [CrossRef]
84. Simmons, H.; Tiwary, P.; Colwell, J.E.; Kontopoulou, M. Improvements in the Crystallinity and Mechanical Properties of PLA by Nucleation and Annealing. *Polym. Degrad. Stab.* **2019**, *166*, 248–257. [CrossRef]
85. Krishnasamy, S.; Ungtrakul, T.; Chandrasekar, M.; Senthil Muthu Kumar, T.; Parameswaranpillai, J.; Mohit, H.; Aravind, D.; Rajini, N.; Siengchin, S.; Natarajan, V. Analysis of the Thermal Properties in Short Sansevieria Cylindrica Fibre/PLA Composites Processed by Twin Screw Extruder Followed by Hot Press Molding Technique. *Mater. Res. Express* **2024**, *11*, 035506. [CrossRef]

86. Hong, J.; Kim, D.S. Preparation and Physical Properties of Polylactide/Cellulose Nanowhisker/Nanoclay Composites. *Polym. Compos.* **2013**, *34*, 293–298. [CrossRef]
87. Li, M.; Li, D.; Deng, Q.; Lin, D.; Wang, Y. Fabrication and Properties of Green Cellulose Nanofibers/Polylactic Acid Composites. *Appl. Mech. Mater.* **2012**, *174–177*, 885–892. [CrossRef]
88. Kuciel, S.; Mazur, K.; Hebda, M. The Influence of Wood and Basalt Fibres on Mechanical, Thermal and Hydrothermal Properties of PLA Composites. *J. Polym. Environ.* **2020**, *28*, 1204–1215. [CrossRef]
89. Bondeson, D.; Oksman, K. Polylactic Acid/Cellulose Whisker Nanocomposites Modified by Polyvinyl Alcohol. *Compos. Part A Appl. Sci. Manuf.* **2007**, *38*, 2486–2492. [CrossRef]
90. Chu, H.; Chen, Z.; Chen, Y.; Wei, D.; Liu, Y.; Zhao, H. Mechanical Properties and Crystallinity of Specific PLA/Cellulose Composites by Surface Modification of Nanofibrillated Cellulose. *Polymers* **2024**, *16*, 2474. [CrossRef] [PubMed]
91. Suryanegara, L.; Nakagaito, A.N.; Yano, H. Thermo-Mechanical Properties of Microfibrillated Cellulose-Reinforced Partially Crystallized PLA Composites. *Cellulose* **2010**, *17*, 771–778. [CrossRef]
92. Mahmoud, Y.; Belhanche-Bensemra, N.; Safidine, Z. Impact of Microcrystalline Cellulose Extracted from Walnut and Apricots Shells on the Biodegradability of Poly (Lactic Acid). *Front. Mater.* **2022**, *9*, 2296–8016. [CrossRef]
93. Niu, Y.; Zhang, X.; He, X.; Zhao, J.; Zhang, W.; Lu, C. Effective Dispersion and Crosslinking in PVA/Cellulose Fiber Biocomposites via Solid-State Mechanochemistry. *Int. J. Biol. Macromol.* **2015**, *72*, 855–861. [CrossRef] [PubMed]
94. Sahu, P.; Gupta, M.K. Water Absorption Behavior of Cellulosic Fibres Polymer Composites: A Review on Its Effects and Remedies. *J. Ind. Text.* **2020**, *51*, 7480S–7512S. [CrossRef]
95. El Assimi, T.; Blažic, R.; Vidović, E.; Raihane, M.; El Meziane, A.; Baouab, M.H.V.; Khouloud, M.; Beniazza, R.; Kricheldorf, H.; Lahcini, M. Polylactide/Cellulose Acetate Biocomposites as Potential Coating Membranes for Controlled and Slow Nutrients Release from Water-Soluble Fertilizers. *Prog. Org. Coat.* **2021**, *156*, 106–255. [CrossRef]
96. Wan Ishak, W.H.; Rosli, N.A.; Ahmad, I. Influence of Amorphous Cellulose on Mechanical, Thermal, and Hydrolytic Degradation of Poly(Lactic Acid) Biocomposites. *Sci. Rep.* **2020**, *10*, 11342. [CrossRef]
97. Xie, L.; Huang, Z.; Meng, H.; Shi, X.; Xie, J. Immunomodulation Effect of Polysaccharides from Liquid Fermentation of *Monascus purpureus* 40269 via Membrane TLR-4 to Activate the MAPK and NF-KB Signaling Pathways. *Int. J. Biol. Macromol.* **2022**, *201*, 480–491. [CrossRef]
98. Trifol, J.; Plackett, D.; Szabo, P.; Daugaard, A.E.; Giacinti Baschetti, M. Effect of Crystallinity on Water Vapor Sorption, Diffusion, and Permeation of PLA-Based Nanocomposites. *ACS Omega* **2020**, *5*, 15362–15369. [CrossRef] [PubMed]
99. Abdulkhani, A.; Hosseinzadeh, J.; Dadashi, S.; Mousavi, M. A Study of Morphological, Thermal, Mechanical and Barrier Properties of PLA Based Biocomposites Prepared with Micro and Nano Sized Cellulosic Fibers. *Cellul. Chem. Technol.* **2015**, *49*, 597–605.
100. Suryanegara, L.; Nakagaito, A.N.; Yano, H. The Effect of Crystallization of PLA on the Thermal and Mechanical Properties of Microfibrillated Cellulose-Reinforced PLA Composites. *Compos. Sci. Technol.* **2009**, *69*, 1187–1192. [CrossRef]

Disclaimer/Publisher's Note: The statements, opinions and data contained in all publications are solely those of the individual author(s) and contributor(s) and not of MDPI and/or the editor(s). MDPI and/or the editor(s) disclaim responsibility for any injury to people or property resulting from any ideas, methods, instructions or products referred to in the content.